

# Deuteron binding energies and form factors from light front field theory

Jason R. Cooke and Gerald A. Miller

*Department of Physics  
University of Washington  
Box 351560  
Seattle WA 98195-1560, USA*

(Dated: October 29, 2018)

## Abstract

The objective of this paper is to investigate how the breaking of manifest rotational invariance in light-front dynamics affects the binding energy and the form factors of the deuteron. To do this, we derive new light-front nucleon-nucleon one- and two-meson-exchange potentials, and use the potentials to solve for the deuteron wave function and binding energy. We find that including two-meson-exchange (TME) potentials partially repairs the broken rotational invariance of the one-meson-exchange (OME) potential. This is shown by a decrease in binding energy difference of different  $m$  states of the deuteron. We calculate the matrix elements of the electromagnetic current using the deuteron wave functions obtained from the OME and OME+TME potentials. Rotational invariance requires that the matrix elements satisfy an angular condition, but in light-front dynamics that condition is only partially satisfied. The current matrix elements from the OME calculation satisfy the angular condition better than the ones from the OME+TME calculation. The matrix elements of the axial current satisfy the angular condition to the same extent regardless of which wave functions are used for the calculation. Finally, we find that at momentum transfers greater than about  $2 \text{ GeV}^2$ , the breaking of rotational invariance causes less uncertainty in the computed deuteron form factors than do the uncertainties in the nucleon form factors.

PACS numbers: 21.45.+v, 03.65.Ge, 03.65.Pm, 11.10.Ef

## I. INTRODUCTION

Recent experiments at Thomas Jefferson National Accelerator Facility have measured the  $A(Q^2)$  structure function of the deuteron for momentum transfers up to 6 (GeV/c)<sup>2</sup> [1], and measurements for  $B(Q^2)$  are planned. Eventually, even higher momentum transfers will be achieved. At such large momentum transfers, a relativistic description of the deuteron is required. Even at lower momentum transfers, a relativistic description is important to understand the details of the form factors. In addition, incorporating relativity is important for the deuteron wave function to transform correctly under boosts to large momentum, which is important for calculating form factors.

One approach that gives a relativistic description of the deuteron is light-front dynamics. The subject of this work is to investigate the consequences of combining light front dynamics with various nuclear models to calculate bound state wave functions, and use them to calculate the deuteron form factors.

The utility of the light-front dynamics was first discussed by Dirac [2]. Light-front dynamics makes use of the light-front coordinate system, where a four-vector  $x^\mu$  is expressed as  $x^\mu = (x^+, x^-, x^1, x^2)$ , with  $x^\pm = x^0 \pm x^3$ . This is simply a change of variables, but an especially convenient one. Using this coordinate system and defining the commutation relations at equal light-front time ( $x^+ = t_{\text{LF}}$ ), we obtain a light-front Hamiltonian [3, 4, 5]. We use Hamiltonian in the light-front Schrödinger equation to solve for bound states. There are many desirable features of the light-front dynamics and the use of light-front coordinates.

First of all, high-energy experiments are naturally described using light-front coordinates. The wave front of a beam of high-energy particles traveling in the (negative) three-direction is defined by a surface where  $x^+$  is (approximately) constant. Such a beam can probe the wave function of a target described in terms of light-front variables [3, 6, 7]: the Bjorken  $x$  variable used to describe high-energy experiments is simply the ratio of the plus momentum of the struck constituent particle to the total plus momentum ( $p^+$ ) of the bound state.

Secondly, the vacuum for a theory with massive particles can be very simple on the light front. This is because all massive particles and anti-particles have positive plus momentum, and the total plus momentum is a conserved quantity. Thus, the naïve vacuum (with  $p^+ = 0$ ) is empty, and diagrams that couple to this vacuum are zero. This greatly reduces the number of non-trivial light-front time-ordered diagrams.

Thirdly, the generators of boosts in the one, two, and plus directions are kinematic, meaning they are independent of the interaction. Thus, even when the Hamiltonian is truncated, the wave functions will transform correctly under boosts. Thus, light-front dynamics is useful for describing form factors at high momentum transfers.

Finally, it is easy to perform relativistic calculations using light-front dynamics. This is partly due to the simplicity of the vacuum, and partly due the the fact that, with light-front variables, center-of-momentum variables can be cleanly separated from the relative momentum variables. This allows us to write relativistic equations which have the simple form of a non-relativistic Schrödinger equation.

One serious drawback of light-front dynamics is that rotational invariance is not manifest in any light-front Hamiltonian [8]. This is a result of selecting a particular direction in space for the orientation of the light-front.

An untruncated light-front Hamiltonian will commute with the total relative angular momentum operator, since the total momentum commutes with the relative momentum. Thus, eigenstates of the full Hamiltonian will also be eigenstates of the angular momentum.

However, as mentioned earlier, a Fock-space truncation of the light-front Hamiltonian results in the momentum operator four-vector losing covariance under rotations. Hence  $J^2$  and the truncated Hamiltonian do not commute and this implies that the eigenstates of the truncated Hamiltonian will not be eigenstates of the angular momentum.

How will this violation of rotational invariance affect physical observables? One way to observe this violation is to note that on the light front, rotational invariance about the  $z$ -axis is maintained. This allows us to classify states as eigenstates of  $J_3$  with eigenvalues  $m$ . We compare the binding energy of deuteron states (which have  $j = 1$ ) with different  $m$  values. If the Hamiltonian were rotationally invariant, the energies should be the same; the breaking of rotational invariance causes the energies to be different [9].

Another symptom of the breaking of rotational invariance is that the angular condition (a relation between the matrix elements of the current, defined in section IV A 4) for the deuteron current is not exactly satisfied [10, 11, 12, 13, 14]. This means that different prescriptions for calculating the deuteron form factors from the deuteron current will in principle give different results when light-front dynamics is used. This dependence on the prescription used has caused concern about the validity of applying light-front dynamics to calculate form factors. We address both the breaking of binding-energy degeneracy and the angular condition in this paper.

One notable feature of this calculation is that it is done entirely with light-front dynamics. The covariant Lagrangian generates light-front potentials, which generate light-front wave functions, which are used in a light-front calculation of the deuteron current and form factors. This is different from other approaches which use deuteron wave functions calculated from equal-time dynamics, then transformed to the light front [10, 11, 12, 13, 14, 15, 16, 17].

We start by introducing a model Lagrangian for nuclear physics which includes chiral symmetry [6] in section II. The methods introduced in Refs. [18, 19] are generalized for use with this nuclear model. The Hamiltonian is derived and used to calculate new light-front nucleon-nucleon one-meson-exchange (OME) and two-meson-exchange (TME) potentials. The notation and conventions defined in the appendix are used extensively in this section. We have some freedom in how to choose the TME potentials, and we consider several different choices.

In section III, the OME and TME potentials are used to calculate the deuteron wave functions and binding energies. We find that by including the TME potentials for the calculation of the deuteron, the binding energy degeneracy is broken by a smaller amount.

The wave functions obtained in section III, are used in section IV to calculate the electromagnetic and axial form factors of the deuteron. Although rotational invariance demands that there be only three independent components of the deuteron current, the light-front calculation of the deuteron current results in four independent components. This is a result of the lack of manifest rotational invariance on the light front. There are several prescriptions for choosing which deuteron current component should be eliminated, and in principle this choice will affect the form factors. We attempt to find currents that transform correctly (or well enough) under rotations so that the choice of “bad” component does not matter too much.

We discuss the results of that search in section V. We find that for most of the currents, the angular condition does not depend strongly on which potential is used to calculate the wave function. The only exception to this is that part of the electromagnetic current which is multiplied by the isoscalar  $F_1$  nucleon form factor satisfies the angular condition much better when using the wave function calculated with the OME potential than with wave function

with other potentials. We also find that the major uncertainty in the calculated deuteron form factors at momentum transfers greater than 2 GeV<sup>2</sup> is due not to the prescription used to determine the form factors from the current, but instead is from the uncertainties in the nucleon form factors.

## II. REALISTIC NUCLEAR MODEL

We consider a nuclear Lagrangian which uses ( $\pi$ ,  $\sigma$ ,  $\rho$ ,  $\omega$ ,  $\eta$ , and  $\delta$ ) for the nucleon-nucleon interaction. This is used to calculate a new light-front nucleon-nucleon potential (LFNN). This model is an extension of the light-front model used by Miller and Machleidt [20]. A new feature of this model is that light-front energy dependent denominators are used in the potentials; the denominators used in Ref. [20] are energy independent.

Note that most of the material covered here can be considered an extension of the work done with the Wick-Cutkosky model in the Refs [18, 19]. This allows us to build upon the previous results.

### A. Model and Formalism

Our starting point is a nuclear Lagrangian [6] which incorporates a non-linear chiral model for the pions. The Lagrangian is based on the linear representations of chiral symmetry used by Gursey [21]. It is invariant (in the limit where  $m_\pi \rightarrow 0$ ) under chiral transformations.

The model prescribes the use of nucleons  $\psi$  (or  $\psi'$ ) and six mesons: the  $\pi$ ,  $\delta$  (also known as the  $a_0(980)$ ),  $\sigma$  (also known as the  $f_0(400 - 1200)$ ),  $\eta$ ,  $\rho$ , and  $\omega$  mesons. The coupling of each meson to the nucleon is governed by the combination of the meson's spin and isospin. The  $\pi$  and  $\eta$  are pseudoscalars, the  $\rho$  and  $\omega$  are vectors, and the  $\delta$  and  $\sigma$  are scalars. Under isospin transformations, the  $\pi$ ,  $\rho$ , and  $\delta$  are isovector particles while the  $\eta$ ,  $\omega$ , and  $\sigma$  are isoscalar particles.

The use of scalar mesons is meant as a simple representation of part of the two-pion-exchange potential which causes much of the medium range attraction between nucleons [22, 23]. It can also be interpreted as the effect of fundamental scalar mesons [24, 25, 26].

The Lagrangian  $\mathcal{L}$  is based on the one used in Refs. [6, 20, 27]. It is given by

$$\begin{aligned} \mathcal{L} = & -\frac{1}{4}\boldsymbol{\rho}^{\mu\nu} \cdot \boldsymbol{\rho}_{\mu\nu} + \frac{m_\rho^2}{2}\boldsymbol{\rho}^\mu \cdot \boldsymbol{\rho}_\mu - \frac{1}{4}\omega^{\mu\nu}\omega_{\mu\nu} + \frac{m_\omega^2}{2}\omega^\mu\omega_\mu \\ & + \frac{1}{4}f^2\text{Tr}(\partial_\mu U \partial^\mu U^\dagger) + \frac{1}{4}m_\pi^2 f^2 \text{Tr}(U + U^\dagger - 2) \\ & + \frac{1}{2}(\partial_\mu\sigma\partial^\mu\sigma - m_\sigma^2\sigma^2) + \frac{1}{2}(\partial_\mu\boldsymbol{\delta} \cdot \partial^\mu\boldsymbol{\delta} - m_\delta^2\boldsymbol{\delta}^2) + \frac{1}{2}(\partial_\mu\eta\partial^\mu\eta - m_\eta^2\eta^2) \\ & + \bar{\psi}' \left[ \gamma^\mu (i\partial_\mu - g_\rho\boldsymbol{\rho}_\mu \cdot \boldsymbol{\tau} - g_\omega\omega_\mu) - U(M + g_\sigma\sigma + g_\delta\boldsymbol{\delta} \cdot \boldsymbol{\tau} + ig_\eta\gamma_5\eta) \right] \psi', \end{aligned} \quad (1)$$

where the bare masses of the nucleon and the mesons are given by  $M$  and  $m_\alpha$  where  $\alpha = \pi, \eta, \sigma, \delta, \rho, \omega$ . We have defined  $V^{\mu\nu} \equiv \partial^\mu V^\nu - \partial^\nu V^\mu$  for  $V = \rho, \omega$ . The unitary matrix  $U$  can be chosen to have one of the three forms  $U_i$ :

$$U_1 \equiv e^{i\gamma_5\boldsymbol{\tau} \cdot \boldsymbol{\pi}/f}, \quad U_2 \equiv \frac{1 + i\gamma_5\boldsymbol{\tau} \cdot \boldsymbol{\pi}/2f}{1 - i\gamma_5\boldsymbol{\tau} \cdot \boldsymbol{\pi}/2f}, \quad U_3 \equiv \sqrt{1 - \pi^2/f^2} + i\gamma_5\boldsymbol{\tau} \cdot \boldsymbol{\pi}/f, \quad (2)$$

which correspond to different definitions of the fields. Note that each of these definitions can be expanded to give

$$U = 1 + i\gamma_5 \frac{\boldsymbol{\tau} \cdot \boldsymbol{\pi}}{f} - \frac{\pi^2}{2f^2} + \mathcal{O}\left(\frac{\pi^3}{f^3}\right). \quad (3)$$

In this work, we consider at most two meson exchange potentials, so we consider  $U$  to be defined by Eq. (3).

In the limit where  $m_\pi \rightarrow 0$ , this Lagrangian, is invariant under the chiral transformation

$$\psi' \rightarrow e^{i\gamma_5 \boldsymbol{\tau} \cdot \mathbf{a}} \psi', \quad U \rightarrow e^{-i\gamma_5 \boldsymbol{\tau} \cdot \mathbf{a}} U e^{-i\gamma_5 \boldsymbol{\tau} \cdot \mathbf{a}}. \quad (4)$$

In this model the other mesons are not affected by the transformation because they are not chiral partners of the pion. This is in contrast to the Lagrangian given in Refs. [6, 27], where the mass and scalar interaction terms for the nucleon were written as  $MU + g_s \phi$  instead of  $U(M + g_s \phi)$ .

## B. Non-interacting Nucleon-Nucleon Theory

The light-front Hamiltonian is derived from this Lagrangian using the same approach used in Refs. [18, 19], the approach used by Miller [6] and others [28, 29, 30, 31]. The basic idea is to write the light-front Hamiltonian ( $P^-$ ) as the sum of a free, non-interacting part and a term containing the interactions. We consider the free part first.

### 1. Free Field Expansions

The solutions for the free fields are similar to those obtained by using equal-time dynamics. In fact, the solutions are formally related by a change of variable, and so the most obvious difference between the two is due to the Jacobian. The field equations have the general form (when Lorentz, spinor, and isospin indices are suppressed) of

$$\alpha(x) = \int \frac{d^2 k_\perp dk^+ \theta(k^+)}{(2\pi)^{3/2} \sqrt{2k^+}} \left[ a_\alpha(\mathbf{k}) e^{-ik^\mu x_\mu} + a_\alpha^\dagger(\mathbf{k}) e^{+ik^\mu x_\mu} \right], \quad (5)$$

where  $\alpha = \pi, \eta, \sigma, \delta, \rho, \omega, \psi$ . Note that in the exponentials,

$$k^\mu x_\mu = \frac{1}{2} (k^+ x^- + k^- x^+) - \mathbf{k}_\perp \cdot \mathbf{x}_\perp. \quad (6)$$

In particular, the solutions for all the mesons and the nucleon field are

$$\boldsymbol{\pi}(x) = \int \frac{d^2 k_\perp dk^+ \theta(k^+)}{(2\pi)^{3/2} \sqrt{2k^+}} \left[ \mathbf{a}_\pi(\mathbf{k}) e^{-ik^\mu x_\mu} + \mathbf{a}_\pi^\dagger(\mathbf{k}) e^{+ik^\mu x_\mu} \right], \quad (7)$$

$$\eta(x) = \int \frac{d^2 k_\perp dk^+ \theta(k^+)}{(2\pi)^{3/2} \sqrt{2k^+}} \left[ a_\eta(\mathbf{k}) e^{-ik^\mu x_\mu} + a_\eta^\dagger(\mathbf{k}) e^{+ik^\mu x_\mu} \right], \quad (8)$$

$$\boldsymbol{\delta}(x) = \int \frac{d^2 k_\perp dk^+ \theta(k^+)}{(2\pi)^{3/2} \sqrt{2k^+}} \left[ \mathbf{a}_\delta(\mathbf{k}) e^{-ik^\mu x_\mu} + \mathbf{a}_\delta^\dagger(\mathbf{k}) e^{+ik^\mu x_\mu} \right], \quad (9)$$

$$\sigma(x) = \int \frac{d^2 k_\perp dk^+ \theta(k^+)}{(2\pi)^{3/2} \sqrt{2k^+}} \left[ a_\sigma(\mathbf{k}) e^{-ik^\mu x_\mu} + a_\sigma^\dagger(\mathbf{k}) e^{+ik^\mu x_\mu} \right], \quad (10)$$

$$\boldsymbol{\rho}^\mu(x) = \int \frac{d^2 k_\perp dk^+ \theta(k^+)}{(2\pi)^{3/2} \sqrt{2k^+}} \sum_{s=1,3} \epsilon^\mu(\mathbf{k}, s) \left[ \mathbf{a}_\rho(\mathbf{k}, s) e^{-ik^\mu x_\mu} + \mathbf{a}_\rho^\dagger(\mathbf{k}, s) e^{+ik^\mu x_\mu} \right], \quad (11)$$

$$\omega^\mu(x) = \int \frac{d^2 k_\perp dk^+ \theta(k^+)}{(2\pi)^{3/2} \sqrt{2k^+}} \sum_{s=1,3} \epsilon^\mu(\mathbf{k}, s) \left[ a_\omega(\mathbf{k}, s) e^{-ik^\mu x_\mu} + a_\omega^\dagger(\mathbf{k}, s) e^{+ik^\mu x_\mu} \right], \quad (12)$$

$$\begin{aligned} \psi(x) = \sqrt{2M} \int \frac{d^2 k_\perp dk^+ \theta(k^+)}{(2\pi)^{3/2} \sqrt{2k^+}} \\ \times \sum_{\lambda=+,-} \sum_{t_3=+,-} \left[ u(\mathbf{k}, \lambda) b(\mathbf{k}) e^{-ik^\mu x_\mu} + v(\mathbf{k}, \lambda) d^\dagger(\mathbf{k}) e^{+ik^\mu x_\mu} \right] \chi_{t_3}. \end{aligned} \quad (13)$$

The polarization vectors are the usual ones. The most general of the commutation relations is

$$\left[ a_{\alpha,i}(\mathbf{k}, s), a_{\beta,j}^\dagger(\mathbf{k}', s') \right] = \delta_{\alpha,\beta} \delta_{i,j} \delta_{s,s'} \delta^{(2,+)}(\mathbf{k} - \mathbf{k}'), \quad (14)$$

where  $\alpha$ ,  $i$ , and  $s$  denote the meson type, isospin, and spin. The anti-commutation relations are

$$\left\{ b(\mathbf{k}, \lambda), b^\dagger(\mathbf{k}', \lambda') \right\} = \left\{ d(\mathbf{k}, \lambda), d^\dagger(\mathbf{k}', \lambda') \right\} = \delta_{\lambda,\lambda'} \delta^{(2,+)}(\mathbf{k} - \mathbf{k}'). \quad (15)$$

All other (anti-)commutation relations vanish. The spinors are normalized so that  $\bar{u}(\mathbf{p}, \lambda') u(\mathbf{p}, \lambda) = \delta_{\lambda'\lambda}$ . For more information on the definition of the spinors, see the Appendix.

## 2. Non-interacting Hamiltonians

The general form of the non-interacting Hamiltonian for each meson is

$$P_0^-(\alpha) = \int d^2 k_\perp dk^+ \theta(k^+) a_\alpha^\dagger(\mathbf{k}) a_\alpha(\mathbf{k}) \frac{k_\perp^2 + m_\alpha^2}{k^+}. \quad (16)$$

For the vector mesons ( $\rho$  and  $\omega$ ), there is an implicit sum over the meson spins. Explicitly, this means that for vector mesons  $a_V^\dagger(\mathbf{k}) a_V(\mathbf{k}) \rightarrow \sum_{s=1,3} a_V^\dagger(\mathbf{k}, s) a_V(\mathbf{k}, s)$ . Likewise, the sum over the isospin of the isovector mesons ( $\pi$ ,  $\delta$ , and  $\rho$ ) is implicit. The sum over isospin can be made explicit by writing  $a_I^\dagger(\mathbf{k}) a_I(\mathbf{k}) \rightarrow \sum_{i=1,3} a_{I,i}^\dagger(\mathbf{k}) a_{I,i}(\mathbf{k})$ . The non-interacting Hamiltonian for the nucleons has a similar form as well,

$$P_0^-(\psi) = \int d^2 k_\perp dk^+ \theta(k^+) \left[ \sum_{\lambda=+,-} b^\dagger(\mathbf{k}, \lambda) b(\mathbf{k}, \lambda) + d^\dagger(\mathbf{k}, \lambda) d(\mathbf{k}, \lambda) \right] \frac{k_\perp^2 + M^2}{k^+}. \quad (17)$$

These equations are what one expects, since a free particle with momenta  $k_\perp$  and  $k^+$  has light-front energy  $k^- = \frac{k_\perp^2 + m^2}{k^+}$ .

### C. Interacting Nucleon-Nucleon Theory

The interaction Hamiltonians are derived from the Lagrangian in Eq. (1) using the techniques presented in Refs. [18, 19]. However, there are some additional complications due to the structure of the interactions.

One complication is that the chiral coupling of the pion field to the nucleons through the  $U$  matrix generates vertices with any number of pions. This is addressed simply by expanding the  $U$  matrix in powers of  $\frac{1}{f}$ , and considering the interaction Hamiltonians order by order.

Another complication is due to the fact that both the vector mesons and the fermions have components which depend on other components of the field [6, 32, 33, 34, 35]. Vector meson fields have four components, but only three degrees of freedom. Likewise, fermion fields have four spinor components, but only two degrees of freedom. When the dependent components are expressed explicitly in terms of the independent components, we obtain new (effective) interaction Hamiltonians for instantaneous vector mesons and fermions. A complete derivation is given by Miller in Ref. [6] and earlier workers cited therein. We illustrate only the main points of the derivation here.

#### 1. Expanding the Pion Interaction

We start by Taylor-expanding  $U$  in powers of  $\frac{1}{f}$ , after which the derivation of the one-meson-interaction Hamiltonian  $P'_{I,1}$  is straightforward. (The prime indicates that it is in terms of  $\psi'$ , not  $\psi$ . We derive the expressions for  $P'_{I,1}$  in the section II C 2.) The result is

$$P'_{I,1} = \int d^2x_{\perp} dx^{-} \bar{\psi}'(x) \left[ g_{\rho} \gamma^{\mu} \rho_{\mu,i}(x) \tau_i + g_{\omega} \gamma^{\mu} \omega_{\mu}(x) + g_{\delta} \delta_i(x) \tau_i + g_{\sigma} \sigma(x) + g_{\pi} (i\gamma_5) \tau_i \pi_i(x) + g_{\chi} (i\gamma_5) \chi(x) \right] \psi'(x). \quad (18)$$

We have defined a dimensionless coupling constant  $g_{\pi} \equiv \frac{M}{f}$ . To save space and to generalize, we define

$$\Gamma_{\alpha} = \begin{cases} i\gamma^5 & \text{if } \alpha \text{ is a pseudoscalar meson } (\pi, \eta) \\ 1 & \text{if } \alpha \text{ is a scalar meson } (\delta, \sigma) \\ \gamma^{\mu} & \text{if } \alpha \text{ is a vector meson } (\rho, \omega) \end{cases} \quad (19)$$

$$T_{\alpha} = \begin{cases} \tau_i & \text{if } \alpha \text{ is an isovector meson } (\pi, \delta, \rho) \\ 1 & \text{if } \alpha \text{ is an isoscalar meson } (\eta, \sigma, \omega) \end{cases} \quad (20)$$

and denote the meson fields by  $\Phi_{\alpha}$ . This allows us to write

$$P'_{I,1} = \sum_{\alpha=\pi,\eta,\sigma,\delta,\rho,\omega} \int d^2x_{\perp} dx^{-} \bar{\psi}'(x) g_{\alpha} \Gamma_{\alpha} T_{\alpha} \Phi_{\alpha}(x) \psi'(x), \quad (21)$$

where the appropriate sums over the meson indices are implicit.

The next step is to derive the two-meson-interaction Hamiltonian which arises from chiral symmetry,  $P'_{I,2c}$ :

$$P'_{I,2c} = \int d^2x_{\perp} dx^{-} \bar{\psi}'(x) \left[ -\frac{g_{\pi}^2}{2M} \tau_i \tau_j \pi_i(x) \pi_j(x) \right]$$

$$\begin{aligned}
& + \frac{g_\pi g_\phi}{M} (i\gamma^5) \tau_i \pi_i(x) \phi(x) \\
& - \frac{g_\pi g_\chi}{M} \tau_i \pi_i(x) \chi(x) \Big] \psi'(x)
\end{aligned} \tag{22}$$

$$= \sum_{\alpha=\pi,\eta,\sigma,\delta} \frac{g_\pi g_\alpha}{M} s_\alpha \int d^2 x_\perp dx^- \bar{\psi}'(x) [\Gamma_\pi T_\pi \Phi_\pi(x)] [\Gamma_\alpha T_\alpha \Phi_\alpha(x)] \psi'(x), \tag{23}$$

where  $s_\alpha$  is a symmetry factor, equal to  $\frac{1}{2}$  when  $\alpha = \pi$ , and 1 otherwise. When the contact interaction is used to calculate diagrams, an additional factor is picked up for the  $\pi\pi$  contact term (due to indistinguishability) which cancels the symmetry factor  $s_\pi$ . Note that this contact interaction involves only scalar and pseudoscalar mesons.

## 2. Elimination of Dependent Fermion Components

We are now ready to express the dependent components of  $\psi'$  in terms of the independent components, and address the problem of instantaneous nucleons. The generation of instantaneous interactions is a general feature of theories with interacting fermions in light-front dynamics. This allows us to use a simplified model to demonstrate how these instantaneous nucleons arise. In particular, we want to postpone the discussion of the complication introduced by the vector mesons until the next section. To this end, we choose to remove all mesons except the  $\sigma$  from the Lagrangian given in Eq. (1). (The  $\sigma$  is chosen since it has the simplest coupling to the nucleon.) The equation of motion for the nucleons is then

$$i\partial\psi' = (M + g_\sigma\sigma)\psi'. \tag{24}$$

Applying the projection operators  $\Lambda_\pm = \frac{1}{2}\gamma^0\gamma^\pm$  (defined in the Appendix) to Eq. (24) splits it into two equations,

$$i\partial^- \psi'_+ = [\boldsymbol{\alpha}_\perp \cdot \mathbf{p}_\perp + \beta(M + g_\sigma\sigma)]\psi'_-, \tag{25}$$

$$i\partial^+ \psi'_- = [\boldsymbol{\alpha}_\perp \cdot \mathbf{p}_\perp + \beta(M + g_\sigma\sigma)]\psi'_+, \tag{26}$$

where  $\psi'_\pm = \Lambda_\pm\psi'$ . This split is useful because in Eq. (24), all four components of the nucleon field are interrelated, while in Eqs. (25) and (26), the two components of  $\psi'_+$  are related to the two components of  $\psi'_-$ , and vice versa.

First, notice that Eq. (25) involves  $\partial^-$ , a dynamic operator in light-front dynamics. Dynamic operators should be avoided since they involve the interaction, and are therefore complicated. We use Eq. (25) to avoid that complication and relate the components of  $\psi$ . Secondly, to keep the relation as simple as possible, we do not attempt to invert the spinor matrix on the right side of Eq. (25). Requiring that the equation for the dependent components be both a kinematic equation and simple equation forces us to choose  $\psi'_+$  as the independent components. The dependent components,  $\psi'_-$ , are defined by

$$\psi'_- = \frac{1}{p^+} [\boldsymbol{\alpha}_\perp \cdot \mathbf{p}_\perp + \beta(M + g_\sigma\sigma)] \psi'_+. \tag{27}$$

Notice that the dependent components consist of a non-interacting part and an interacting part. We separate these parts by defining  $\psi$  (without a prime) to be the free nucleon field, and  $\xi$  to be the part of  $\psi'$  that is due to interactions. So

$$\psi' = \psi + \xi, \tag{28}$$



where

$$\xi = \xi_- = \frac{1}{p^+} \beta(g_\sigma \sigma) \psi_+ = \frac{\gamma^+}{2p^+} (g_\sigma \sigma) \psi_+. \quad (29)$$

This allows us to write

$$\psi' = \psi + \frac{\gamma^+}{2p^+} (g_\sigma \sigma) \psi_+ \quad (30)$$

$$= \psi + \frac{\gamma^+}{2p^+} (g_\sigma \sigma) \psi' \quad (31)$$

The last equation follows is obtained from noting that  $(\gamma^+)^2 = 0$ , which implies that  $\gamma^+ \psi' = \gamma^+ \psi_+$ .

Plugging Eq. (31) into Eq. (18) and removing all mesons except the  $\sigma$  meson, we obtain

$$P'_{I,1}^- = P_{I,1}^- + P_{I,2}^-, \quad (32)$$

$$P_{I,1}^- = \int d^2 x_\perp dx^- \bar{\psi}(x) g_\sigma \sigma(x) \psi(x), \quad (33)$$

$$P_{I,2}^- = \int d^2 x_\perp dx^- \bar{\psi}(x) \left[ g_\sigma \sigma(x) \frac{\gamma^+}{2p^+} g_\sigma \sigma(x) \right] \psi(x). \quad (34)$$

We interpret the  $\frac{\gamma^+}{2p^+}$  factor as a type of nucleon propagator that joins any two meson interactions (although having two of these propagators adjacent to each other causes the interaction to vanish since  $(\gamma^+)^2 = 0$ ). Because this propagator does not allow for an energy denominator (as it is already between two potentials),  $\frac{\gamma^+}{2p^+}$  is called an *instantaneous* propagator.

Thus, when constructing the diagrams for the light-front potentials, we must also include instantaneous propagators for the nucleons in addition to the usual propagators.

### 3. Elimination of Dependent Vector Meson Components

Like the nucleons, the vector mesons have a dependent component that contains interactions and must be eliminated. This process is complicated somewhat by the fact that the dependent nucleon components must be eliminated at the same time. The salient points of the combined elimination of the dependent nucleon and vector meson components are discussed in detail by Miller [6].

The result is that the vector meson field must be redefined and an instantaneous vector meson propagator is generated in addition to an instantaneous nucleon propagator. However, when the nucleon-nucleon potential is calculated, the redefinition of the vector meson field exactly cancels the contribution of the instantaneous vector meson. The result is that the potentials can formally be calculated using the original vector meson field.

In this work, we use that result to simplify our derivations of nucleon-nucleon potentials by formally using the naïve form of the vector meson field. Thus, we find an interaction Hamiltonian similar to the one shown in Eq. (34),

$$P'_{I,1}^- = P_{I,1}^- + P_{I,2}^-, \quad (35)$$

$$P_{I,1}^- = \sum_{\alpha=\pi,\eta,\sigma,\delta,\rho,\omega} \int d^2x_\perp dx^- \bar{\psi}(x) g_\alpha \Gamma_\alpha T_\alpha \Phi_\alpha(x) \psi(x), \quad (36)$$

$$P_{I,2}^- = \sum_{\alpha_1,\alpha_2=\pi,\eta,\sigma,\delta,\rho,\omega} \int d^2x_\perp dx^- \bar{\psi}(x) [g_{\alpha_1} \Gamma_{\alpha_1} T_{\alpha_1} \Phi_{\alpha_1}(x)] \frac{\gamma^+}{2p^+} [g_{\alpha_2} \Gamma_{\alpha_2} T_{\alpha_2} \Phi_{\alpha_2}(x)] \psi(x). \quad (37)$$

We may continue to interpret  $\frac{\gamma^+}{2p^+}$  as an instantaneous nucleon propagator, since in the derivation in Ref. [6] it is clear that the potential vanishes when there are two adjacent instantaneous propagators. In Refs. [6, 20], sign of the coupling of the vector mesons in the equations equivalent to Eq. (37) has the wrong sign; the coupling of the mesons in Eq. (37) must be the same as in Eq. (36).

Also note that in principle the same prescription has to be applied to the contact interaction, although to the order of two mesons, this simply has the effect of removing the primes. We find that

$$P_{I,2c}^- = \sum_{\alpha=\pi,\eta,\sigma,\delta} \frac{s_\alpha}{M} \int d^2x_\perp dx^- \bar{\psi}(x) [g_\pi \Gamma_\pi T_\pi \Phi_\pi(x)] [g_\alpha \Gamma_\alpha T_\alpha \Phi_\alpha(x)] \psi(x). \quad (38)$$

Note that  $P_{I,2c}^-$  and  $P_{I,2}^-$  have forms that are very similar. In fact, we can obtain  $P_{I,2c}^-$  from  $P_{I,2}^-$  by making the following changes:

1. Replace  $\frac{\gamma^+}{2p^+}$  with  $\frac{s_\alpha}{M}$ .
2. Replace  $\alpha_1$  with  $\pi$ .
3. Restrict the sum on  $\alpha_2$  to  $\pi, \eta, \sigma, \delta$ .

#### 4. Interaction Hamiltonians in Momentum Space

We look at the matrix element of the interaction Hamiltonians between initial and final states given by  $|k_i, \lambda_i, \tau_i\rangle = b^\dagger(k_i, \lambda_i) \chi_{\tau_i} |0\rangle$  and  $\langle k_f, \lambda_f, \tau_f| = \langle 0| b(k_f, \lambda_f) \chi_{\tau_f}^\dagger$  where both the bra and the ket have units of  $[M^{-3/2}]$ . We find that

$$P_{I,1}^-(f, i) = \sum_{\alpha=\pi,\eta,\sigma,\delta,\rho,\omega} \frac{g_\alpha 2M}{2(2\pi)^3 \sqrt{k_f^+ k_i^+}} \int \frac{d^2q_\perp dq^+ \theta(q^+)}{\sqrt{2(2\pi)^3} \sqrt{q^+}} \bar{u}(\mathbf{k}_f, \lambda_f) \Gamma_\alpha u(\mathbf{k}_i, \lambda_i) \chi_{\tau_f}^\dagger T_\alpha \chi_{\tau_i} \int d^2x_\perp dx^- e^{+ik_f^\mu x_\mu} e^{-ik_i^\mu x_\mu} [a_\alpha(\mathbf{q}) e^{-iq^\mu x_\mu} + a_\alpha^\dagger(\mathbf{q}) e^{+iq^\mu x_\mu}] F_\alpha(\mathbf{q}), \quad (39)$$

where  $\mathbf{q} = (q^+, \mathbf{q}_\perp)$  and there are implicit  $\theta$ -functions on  $q^+$  for each particle to ensure that the light-front energy is positive. These are occasionally suppressed to simplify the equations. We include a meson-nucleon form factor  $F_\alpha$  to phenomenologically account for the fact that the mesons and nucleons are composite objects.

Now, we evaluate  $P^-$  at  $x^+ = 0$  and use

$$\int d^2x_\perp dx^- e^{i(k_f - k_i - q)^\mu x_\mu} = 2(2\pi)^3 \delta^{(2,+)}(k_f - k_i - q), \quad (40)$$

to write

$$P_{I,1}^-(f, i) = \sum_{\alpha=\pi,\eta,\sigma,\delta,\rho,\omega} g_\alpha 2M \frac{\bar{u}(\mathbf{k}_f, \lambda_f) \Gamma_\alpha u(\mathbf{k}_i, \lambda_i)}{\sqrt{2(2\pi)^3} \sqrt{k_f^+ k_i^+ q^+}} \chi_{\tau_f}^\dagger T_\alpha \chi_{\tau_i} \left[ a_\alpha(\mathbf{q}) \theta(k_f^+ - k_i^+) + a_\alpha^\dagger(\mathbf{q}) \theta(-(k_f^+ - k_i^+)) \right] F_\alpha(\mathbf{q}). \quad (41)$$

We define  $\mathbf{q} = \text{sign}(k_f^+ - k_i^+) (\mathbf{k}_f - \mathbf{k}_i)$ , which ensures that the  $q^+$  of the meson is positive.

Next we consider the two-meson interactions. First take the interaction with the instantaneous propagator given by Eq. (37). Plugging in the field definitions gives

$$\begin{aligned} P_{I,2}^-(f, i) &= \sum_{\alpha_1, \alpha_2=\pi,\eta,\sigma,\delta,\rho,\omega} \frac{g_{\alpha_1} g_{\alpha_2} 2M}{2(2\pi)^3 \sqrt{k_f^+ k_i^+}} \int \frac{d^2 q_{1\perp} dq_1^+ \theta(q_1^+)}{(2\pi)^{3/2} \sqrt{2q_1^+}} \int \frac{d^2 q_{2\perp} dq_2^+ \theta(q_2^+)}{(2\pi)^{3/2} \sqrt{2q_2^+}} \\ &\quad \frac{\theta(k_m^+)}{2k_m^+} \bar{u}(\mathbf{k}_f, \lambda_f) \Gamma_{\alpha_2} \gamma^+ \Gamma_{\alpha_1} u(\mathbf{k}_i, \lambda_i) \chi_{\tau_f}^\dagger T_{\alpha_2} T_{\alpha_1} \chi_{\tau_i} \\ &\quad \int d^2 x_\perp dx^- e^{+ik_f^\mu x_\mu} e^{-ik_i^\mu x_\mu} \left[ a_{\alpha_2}(\mathbf{q}_2) e^{-iq_2^\mu x_\mu} + a_{\alpha_2}^\dagger(\mathbf{q}_2) e^{+iq_2^\mu x_\mu} \right] F_{\alpha_2}(\mathbf{q}_2) \\ &\quad \left[ a_{\alpha_1}(\mathbf{q}_1) e^{-iq_1^\mu x_\mu} + a_{\alpha_1}^\dagger(\mathbf{q}_1) e^{+iq_1^\mu x_\mu} \right] F_{\alpha_1}(\mathbf{q}_1) \quad (42) \\ &= \sum_{\alpha_1, \alpha_2=\pi,\eta,\sigma,\delta,\rho,\omega} g_{\alpha_1} g_{\alpha_2} 2M \frac{\bar{u}(\mathbf{k}_f, \lambda_f) \Gamma_{\alpha_2} \gamma^+ \Gamma_{\alpha_1} u(\mathbf{k}_i, \lambda_i)}{2(2\pi)^3 \sqrt{k_f^+ k_i^+}} \\ &\quad \left[ \chi_{\tau_f}^\dagger T_{\alpha_2} T_{\alpha_1} \chi_{\tau_i} \right] \int \frac{d^2 k_{m\perp} dk_m^+ \theta(k_m^+)}{2k_m^+ \sqrt{q_1^+ q_2^+}} \\ &\quad \left[ a_{\alpha_2}(k_f - k_m) \theta(k_f^+ - k_m^+) + a_{\alpha_2}^\dagger(k_m - k_f) \theta(k_m^+ - k_f^+) \right] F_{\alpha_2}(\mathbf{q}_2) \\ &\quad \left[ a_{\alpha_1}(k_m - k_i) \theta(k_m^+ - k_i^+) + a_{\alpha_1}^\dagger(k_i - k_m) \theta(k_i^+ - k_m^+) \right] F_{\alpha_1}(\mathbf{q}_1) \quad (43) \end{aligned}$$

Note that the momenta  $q_1$  and  $q_2$  are implicitly functions of the momenta  $k_f$ ,  $k_m$ , and  $k_i$ .

We could also write out the contact interaction given by Eq. (38) in momentum space, but it is related to Eq. (43) by replacing  $\frac{\theta(p^+) \gamma^+}{2p^+}$  with  $\frac{s_\alpha}{M}$  and restricting the allowed values of the  $\alpha$ 's.

#### D. Feynman Rules for Nucleon-Nucleon Potentials

Now that we have the one-meson- and two-meson-exchange expressed in momentum space, we are now ready to write out the Feynman rules for diagrams in our model. For simplicity, the only diagrams considered are those where a meson emitted by one nucleon is absorbed by the other nucleon. Since we are only interested in the two-nucleon to two-nucleon potentials, we follow the same approach as outlined in Ref. [19] to derive the rules. We denote a ‘‘normal’’ nucleon propagator by a solid line with an arrow, an instantaneous nucleon propagator by a solid line with a stroke across it, mesons of all type by a dashed line, and energy denominator terms by a vertical, light, dotted line.

1. Overall factor of  $\frac{4M^2 \delta^{\perp,+}(P_f - P_i)}{2(2\pi)^3 \sqrt{k_{1f}^+ k_{2f}^+ k_{1i}^+ k_{2i}^+}}$ .
2. Usual light-front rules for  $p_\perp$  and  $p^+$  momentum conservation.

3. Factor of  $\frac{\theta(q_i)}{q_i}$  for each internal line, including any instantaneous nucleon lines.
4. A factor of  $\frac{1}{P^- - \sum_i q_i^-}$  for each energy denominator.
5. Each meson connects the two nucleons, and each end of the meson line has a factor of  $g_\alpha \Gamma_\alpha T_\alpha F_\alpha(q)$ . The indices of the isospin factors on each end of the meson are contracted together. The Lorentz indices of the gamma matrices are contracted with  $-g^{\mu\nu}$  for the vector mesons.
6. For each contact vertex, multiply by a factor of  $\frac{1}{M}$ . If the vertex is a  $\pi - \pi$  vertex, symmetrize the  $T_\pi T_\pi = \tau_i \tau_j$  by replacing it with  $\delta_{i,j}$ .
7. Factor of  $\frac{k^+ M}{2M} = \sum_\lambda u(k, \lambda) \bar{u}(k, \lambda)$  for each propagating nucleon and  $\frac{\gamma^+}{2}$  for an instantaneous nucleon.
8. Integrate with  $4M^2 \int \frac{d^2 k_\perp dk^+}{2(2\pi)^3}$  over any internal momentum loops.
9. Put the spinor factors for nucleon 1 and 2 between  $\bar{u}u$ 's and the isospin factors between the initial and final state isospin.

From this list, it is useful to summarize what needs to be done to convert a graph with an instantaneous nucleon to one with a contact interaction:

1. Replace  $\frac{\theta(k^+) \gamma^+}{k^+}$  with  $\frac{1}{M}$ .
2. If both mesons are pions, replace  $T_i T_j$  with  $\delta_{i,j}$ .

These rules make it easy to write down what various potentials are.

## E. Nucleon-Nucleon Potentials

The meson exchange potentials have the same basic form as in Refs. [18, 19], however we must include the contact interaction and instantaneous nucleon propagators for the nuclear model used here. First, we discuss how to include the contact diagrams from the standpoint of the Bethe-Salpeter equation, then we begin to calculate the light-front potentials.

### 1. The Bethe-Salpeter Equation and Chiral Symmetry

The kernel of the Bethe-Salpeter equation [36, 37, 38, 39, 40] for this nuclear model is richer than the one presented in Refs. [19] for the Wick-Cutkosky model. This is due mainly to the presence of the contact interactions which are generated by the chirally invariant coupling of the pion to the nucleon. Several of the lowest-order pieces of the full kernel  $K$  are shown in Fig. 1. (Note that for Feynman diagrams, it is useful to combine the “normal” nucleon propagator with the instantaneous nucleon propagator [41, 42, 43], and denote the combination with a solid line.)

As discussed in Refs. [18, 19], each of these Feynman diagrams is covariant. This means that we may choose any of the diagrams from  $K$  to construct a new kernel  $K'$ , and the infinite series of potential diagrams physically equivalent to  $K'$  will also be covariant.

In practice, this means that when deciding which two-meson-exchange potentials to include for calculating the deuteron wave function, we may neglect the crossed diagrams. Although including only the box and contact two-meson-exchange diagrams may affect the exact binding energy calculated, we should find a partial restoration of rotational invariance. We reiterate that the focus of this work is on understanding the effects of the breaking of rotational invariance and how to restore it; our goal is not precise agreement with experimental results.

We also want to keep the potentials chirally symmetric as well. Whereas Lorentz symmetry is maintained by using a kernel with any Feynman diagrams (with potentially arbitrary coefficients), chiral symmetry relates the strength of the  $\pi\pi$  contact interaction to the strength of the pion-nucleon coupling.

Chiral symmetry tells us that for pion-nucleon scattering at threshold, the sum of the time-ordered graphs approximately cancels [6]. Furthermore, upon closer examination, we find that all the light-front time-ordered graphs for the scattering amplitude vanish except for the two graphs with instantaneous nucleons and the contact graph. These graphs are shown in Fig. 2. Using the Feynman rules, and denoting the nucleon momentum by  $k$  and the pion momentum by  $q$ , we find that

$$\mathcal{M}_U = C \frac{\tau_i \tau_j}{2(k^+ + q^+)} u(k') \gamma^+ u(k), \quad (44)$$

$$\mathcal{M}_X = C \frac{\tau_j \tau_i}{2(k^+ - q^+)} u(k') \gamma^+ u(k), \quad (45)$$

$$\mathcal{M}_C = C \frac{-\delta_{i,j}}{M} u(k') u(k), \quad (46)$$

where the factors common to all amplitudes are denoted by  $C$ .

For threshold scattering, we take  $k = k' = M$  and  $q = q' = m_\pi$ . In that limit, we find

$$\mathcal{M}_U = C' \frac{\delta_{i,j} + i\epsilon_{i,j,k} \tau_k}{2(M + m_\pi)}, \quad (47)$$

$$\mathcal{M}_X = C' \frac{\delta_{i,j} - i\epsilon_{i,j,k} \tau_k}{2(M - m_\pi)}, \quad (48)$$

$$\mathcal{M}_C = C' \frac{-\delta_{i,j}}{M}, \quad (49)$$

where  $C' = C \bar{u}(k') u(k)$ . In the limit that  $m_\pi \rightarrow 0$ , the sum of these three terms vanishes. The term in these equations proportional to  $\tau_k$  is the famous Weinberg-Tomazowa term [44, 45].

The fact that the amplitudes cancel only when the contact interaction is included demonstrates that chiral symmetry can have a significant effect on calculations. In terms of two-pion-exchange potentials, this result means that the contact potentials cancel strongly with both the iterated box potentials and the crossed potentials. This serves to reduce the strength of the total two-pion-exchange potential, which should lead to more stable results.

However, since we do not use the crossed graphs for the nucleon-nucleon potential, we must come up with a prescription which divided the contact interactions into two parts which cancel the box and crossed diagrams separately. We do this by formally defining two new contact interactions, so that

$$\mathcal{M}_{C_U} \equiv \frac{M}{2(M + m_\pi)} \mathcal{M}_C, \quad (50)$$

$$\mathcal{M}_{C_X} \equiv \mathcal{M}_C - \mathcal{M}_{C_U}. \quad (51)$$

With these definitions, we find that at threshold and in the chiral limit,

$$\mathcal{M}_U + \mathcal{M}_{C_U} = 0, \quad (52)$$

$$\mathcal{M}_X + \mathcal{M}_{C_X} = 0. \quad (53)$$

This indicates that we can incorporate approximate chiral symmetry without including crossed graphs simply by weighting each graph with a contact interaction by a factor of  $\frac{M}{2(M+m_\pi)}$ .

## 2. OME Potential

The one meson exchange (OME) potential connects an initial state with two nucleons to a final state with two nucleons, has one meson in the intermediate state, and has the meson emitted and absorbed by different nucleons. With these restrictions, along with the fact that in light-front dynamics the interaction does not allow for particles to be created from the vacuum, we find that there each meson has only two diagrams for the OME potential. These diagrams are shown in Fig. 3.

The Feynman rules derived in the previous section are used to derive the potential for these diagrams. We factor out an overall factor of  $\frac{4M^2\delta(k_{1f}+k_{2f}-k_{1i}-k_{2i})}{2\sqrt{k_{1f}^+k_{1i}^+k_{2f}^+k_{2i}^+}}$  that is common to all the two-nucleon potentials and suppress it from now on. Then we get

$$V_{\text{OME},\alpha} = \frac{g_\alpha^2 \mathbf{T}_{\alpha,1} \cdot \mathbf{T}_{\alpha,2}}{(2\pi)^3} \bar{u}(\mathbf{k}_{1f}, \lambda_{1f}) \Gamma_\alpha u(\mathbf{k}_{1i}, \lambda_{1i}) \bar{u}(\mathbf{k}_{2f}, \lambda_{2f}) \Gamma_\alpha u(\mathbf{k}_{2i}, \lambda_{2i}) F_\alpha^2(\mathbf{q})$$

$$\left[ \frac{\theta(k_{1f}^+ - k_{1i}^+)}{(k_{1f}^+ - k_{1i}^+)(P^- - k_{1i}^- - k_{2f}^-) - m_\alpha^2 - (k_{1i,\perp} - k_{1f,\perp})^2} + \frac{\theta(k_{1i}^+ - k_{1f}^+)}{(k_{1i}^+ - k_{1f}^+)(P^- - k_{1f}^- - k_{2i}^-) - m_\alpha^2 - (k_{1i,\perp} - k_{1f,\perp})^2} \right]. \quad (54)$$

In the scattering regime ( $P^- = k_{1f}^- + k_{2f}^- = k_{1i}^- + k_{2i}^-$ ), Eq. (54) agrees with Eq. (4.7) in Ref. [6], after taking into account the difference in spinor normalization (we use  $\bar{u}u = 1$ ).

To simplify the potential, we define

$$a = \left[ \theta(k_{1f}^+ - k_{1i}^+) \times (k_{1f}^+ - k_{1i}^+)(P^- - k_{1i}^- - k_{2f}^-) + \theta(k_{1i}^+ - k_{1f}^+) \times (k_{1i}^+ - k_{1f}^+)(P^- - k_{1f}^- - k_{2i}^-) \right] - k_{i,\perp}^2 - k_{f,\perp}^2, \quad (55)$$

$$b = 2k_{i,\perp} k_{f,\perp}, \quad (56)$$

so

$$V_{\text{OME},\alpha} = \frac{g_\alpha^2 \mathbf{T}_{\alpha,1} \cdot \mathbf{T}_{\alpha,2}}{(2\pi)^3} F_\alpha(\mathbf{q})^2 \frac{\bar{u}(\mathbf{k}_{1f}, \lambda_{1f}) \Gamma_\alpha u(\mathbf{k}_{1i}, \lambda_{1i}) \bar{u}(\mathbf{k}_{2f}, \lambda_{2f}) \Gamma_\alpha u(\mathbf{k}_{2i}, \lambda_{2i})}{[a - m_\alpha^2 + b \cos(\phi_f - \phi_i)]}. \quad (57)$$

Now we consider the precise form to use for the meson-nucleon form factor. We assume that it has a  $n$ -pole form [22], so that the denominator of the meson-nucleon form factor has the same form as the denominator of the potential in the scattering regime. In particular,  $\Lambda_\alpha$

playing the role of  $m_\alpha$  for the form factor. For simplicity, we declare that the denominator of the form factor always has the same form of the denominator of the potential. Thus,

$$F_\alpha(\mathbf{q}) = \left( \frac{\Lambda_\alpha^2 - m_\alpha^2}{a - \Lambda_\alpha^2 + b \cos(\phi_f - \phi_i)} \right)^{n_\alpha}. \quad (58)$$

Inserting the explicit expression of for the meson-nucleon form factor into the potential results in

$$V_{\text{OME},\alpha} = \frac{g_\alpha^2 \mathbf{T}_{\alpha,1} \cdot \mathbf{T}_{\alpha,2}}{(2\pi)^3} (\Lambda_\alpha^2 - m_\alpha^2)^{2n_\alpha} \frac{\bar{u}(\mathbf{k}_{1f}, \lambda_{1f}) \Gamma_\alpha u(\mathbf{k}_{1i}, \lambda_{1i}) \bar{u}(\mathbf{k}_{2f}, \lambda_{2f}) \Gamma_\alpha u(\mathbf{k}_{2i}, \lambda_{2i})}{[a - m_\alpha^2 + b \cos(\phi_f - \phi_i)] [a - \Lambda_\alpha^2 + b \cos(\phi_f - \phi_i)]^{2n_\alpha}}. \quad (59)$$

Now, since the light-front potentials have exact rotational invariance about the  $z$ -axis, they conserve the  $J_z$  quantum number  $m$ . Thus, these potentials connect only states with the same value of  $m$ . This means that, in general, light-front potentials may be written as

$$V(\phi_f, \phi_i) = \sum_{m=-\infty}^{\infty} e^{im(\phi_i - \phi_f)} V^m, \quad (60)$$

where  $V^m$  is the potential in the magnetic quantum number basis. This relation can be inverted to obtain  $V^m$  in terms of  $V(\phi_f, \phi_i)$ ,

$$V_{\text{OME},\alpha}^m = \frac{g_\alpha^2 \mathbf{T}_{\alpha,1} \cdot \mathbf{T}_{\alpha,2}}{(2\pi)^3} (\Lambda_\alpha^2 - m_\alpha^2)^{2n_\alpha} \int \frac{d\phi_f}{2\pi} e^{im\phi_f} \frac{[\bar{u}(\mathbf{k}_{1f}, \lambda_{1f}) \Gamma_\alpha u(\mathbf{k}_{1i}, \lambda_{1i}) \bar{u}(\mathbf{k}_{2f}, \lambda_{2f}) \Gamma_\alpha u(\mathbf{k}_{2i}, \lambda_{2i})]_{\phi_i=0}}{[a - m_\alpha^2 + b \cos(\phi_f)] [a - \Lambda_\alpha^2 + b \cos(\phi_f)]^{2n_\alpha}}. \quad (61)$$

To continue on, we need to get an expression for  $\phi_f$  dependence the  $\bar{u}u$  matrix elements. These are calculated in Ref. [46]. Summarizing, we can write

$$\bar{u}(\mathbf{k}_{1f}, \lambda_{1f}) \Gamma_\alpha u(\mathbf{k}_{1i}, \lambda_{1i}) \bar{u}(\mathbf{k}_{2f}, \lambda_{2f}) \Gamma_\alpha u(\mathbf{k}_{2i}, \lambda_{2i}) = \sum_j C_j(\Gamma_\alpha, \Gamma_\alpha) e^{ij\phi_f}, \quad (62)$$

where the  $C$  depends implicitly on all the variables on the left-hand side except  $\phi_f$  and  $\phi_i$ . Thus,

$$V_{\text{OME},\alpha}^m = g_\alpha^2 (\mathbf{T}_{\alpha,1} \cdot \mathbf{T}_{\alpha,2}) \frac{(\Lambda_\alpha^2 - m_\alpha^2)^{2n_\alpha}}{(2\pi)^3} \sum_j C_j(\Gamma_\alpha, \Gamma_\alpha) \int \frac{d\phi_f}{2\pi} \frac{e^{i(m+j)\phi_f}}{[a - m_\alpha^2 + b \cos(\phi_f)] [a - \Lambda_\alpha^2 + b \cos(\phi_f)]^{2n_\alpha}}. \quad (63)$$

The cosine integral is denoted by  $I$ , and is calculated in Ref. [46]. Substituting  $I$  for the integral, we obtain

$$V_{\text{OME},\alpha}^m = g_\alpha^2 (\mathbf{T}_{\alpha,1} \cdot \mathbf{T}_{\alpha,2}) \frac{(\Lambda_\alpha^2 - m_\alpha^2)^{2n_\alpha}}{(2\pi)^3} \sum_j C_j(\Gamma_\alpha, \Gamma_\alpha) I(m+j, a - m_\alpha^2, 1, a - \Lambda_\alpha^2, 2n_\alpha, b). \quad (64)$$

All of the terms in Eq. (64) are known, and the potential can now be calculated numerically.

### 3. TME Potentials

We two-meson-exchange (TME) potentials consider here are the box diagrams (see Fig. 4) and the contact diagrams (see Fig. 5). We do not consider the crossed diagrams because they are not needed to restore rotational invariance, as shown in section II E 1.

### 4. Stretched Box Potential

We use the Feynman rules to write the stretched-box potential shown in Fig. 4(b),

$$\begin{aligned}
V_{\text{TME:SB}}^{\alpha_f, \alpha_i} &= \frac{g_{\alpha_f}^2 g_{\alpha_i}^2 4M^2 [\mathbf{T}_{\alpha_f,1} \cdot \mathbf{T}_{\alpha_f,2}] [\mathbf{T}_{\alpha_i,1} \cdot \mathbf{T}_{\alpha_i,2}]}{(2\pi)^3} \int \frac{d^2 k_{2m\perp} dk_{2m}^+}{2(2\pi)^3 k_{1m}^+ k_{2m}^+} \\
&\quad {}_{1f} \langle \left( \Gamma_{\alpha_f} \frac{k_{1m} + M}{2M} \Gamma_{\alpha_i} \right) \rangle_{1m} \times {}_{2f} \langle \left( \Gamma_{\alpha_f} \frac{k_{2m} + M}{2M} \Gamma_{\alpha_i} \right) \rangle_{2m} \\
&\quad \theta(k_{1m}^+) \theta(k_{2m}^+) \theta(k_{2i}^+ - k_{2m}^+) \theta(k_{2m}^+ - k_{2f}^+) \\
&\quad \frac{F_{\alpha_f}(\mathbf{q}_f)^2}{(k_{2m}^+ - k_{2f}^+) (P^- - k_{1m}^- - k_{2f}^-) - m_{\alpha_f}^2 - (\mathbf{k}_{1f\perp} - \mathbf{k}_{1m\perp})^2} \\
&\quad \frac{1}{P^- - k_{1i}^- - k_{2f}^- - q_f^- - q_i^-} \\
&\quad \frac{F_{\alpha_i}(\mathbf{q}_i)^2}{(k_{2i}^+ - k_{2m}^+) (P^- - k_{1i}^- - k_{2m}^-) - m_{\alpha_i}^2 - (\mathbf{k}_{1m\perp} - \mathbf{k}_{1i\perp})^2} \\
&\quad + \{1 \leftrightarrow 2\}.
\end{aligned} \tag{65}$$

To compress notation, we defined  ${}_{1f} \langle \equiv \bar{u}(\mathbf{k}_{1f}, \lambda_{1f})$ ,  $\rangle_{1i} \equiv u(\mathbf{k}_{1i}, \lambda_{1i})$ , and so on. The symbol  $\{1 \leftrightarrow 2\}$  means that all labels 1 are replaced with 2 and vice versa. This is a way of explicitly stating the potential is invariant under exchange of nucleons 1 and 2.

We also used the following relation to simplify this expression:

$$\begin{aligned}
&\sum_{\tau_{2m}} \chi_{\tau_{2f}}^\dagger T_{\alpha_f, j} \chi_{\tau_{2m}} \chi_{\tau_{2m}}^\dagger T_{\alpha_i, i} \chi_{\tau_{2i}} \chi_{\tau_{1f}}^\dagger T_{\alpha_f, j} \chi_{\tau_{1m}} \chi_{\tau_{1m}}^\dagger T_{\alpha_i, i} \chi_{\tau_{1i}} \\
&= \langle \tau_f | [\mathbf{T}_{\alpha_f,1} \cdot \mathbf{T}_{\alpha_f,2}] [\mathbf{T}_{\alpha_i,1} \cdot \mathbf{T}_{\alpha_i,2}] | \tau_i \rangle \\
&= [\mathbf{T}_{\alpha_f,1} \cdot \mathbf{T}_{\alpha_f,2}] [\mathbf{T}_{\alpha_i,1} \cdot \mathbf{T}_{\alpha_i,2}].
\end{aligned} \tag{66}$$

### 5. Mesa Potential

We consider the Mesa potential next,  $V_{\text{TME:M}}$ , shown in Fig. 4(a). Using the Feynman rules results in

$$\begin{aligned}
V_{\text{TME:M}}^{\alpha_f, \alpha_i} &= \frac{g_{\alpha_f}^2 g_{\alpha_i}^2 4M^2 [\mathbf{T}_{\alpha_f,1} \cdot \mathbf{T}_{\alpha_f,2}] [\mathbf{T}_{\alpha_i,1} \cdot \mathbf{T}_{\alpha_i,2}]}{(2\pi)^3} \int \frac{d^2 k_{2m\perp} dk_{2m}^+}{2(2\pi)^3 k_{1m}^+ k_{2m}^+} \\
&\quad {}_{1f} \langle \left( \Gamma_{\alpha_f} \frac{\gamma^+}{2} \Gamma_{\alpha_i} \right) \rangle_{1m} \times {}_{2f} \langle \left( \Gamma_{\alpha_f} \frac{k_{2m} + M}{2M} \Gamma_{\alpha_i} \right) \rangle_{2m} \\
&\quad \theta(k_{1m}^+) \theta(k_{2m}^+) \theta(k_{2i}^+ - k_{2m}^+) \theta(k_{2m}^+ - k_{2f}^+)
\end{aligned}$$



$$\begin{aligned}
& \frac{F_{\alpha_f}(\mathbf{q}_f)^2}{(k_{2f}^+ - k_{2m}^+)(P^- - k_{1f}^- - k_{2m}^-) - m_{\alpha_f}^2 - (\mathbf{k}_{1f\perp} - \mathbf{k}_{1m\perp})^2} \frac{1}{2M} \\
& \frac{F_{\alpha_i}(\mathbf{q}_i)^2}{(k_{2i}^+ - k_{2m}^+)(P^- - k_{1i}^- - k_{2m}^-) - m_{\alpha_i}^2 - (\mathbf{k}_{1m\perp} - \mathbf{k}_{1i\perp})^2} \\
& + \{1 \leftrightarrow 2\}.
\end{aligned} \tag{67}$$

## 6. Contact Potential

The last potential we will calculate explicitly is the contact potential  $V_{\text{TME:C}}$ , shown in Fig. 5(a). The rules relate this potential to  $V_{\text{TME:M}}$  in a simple fashion. If both the initial and final mesons are not pions, then the potential is

$$\begin{aligned}
V_{\text{TME:C}}^{\alpha_f, \alpha_i} &= \frac{g_{\alpha_f}^2 g_{\alpha_i}^2 4M^2 [\mathbf{T}_{\alpha_f,1} \cdot \mathbf{T}_{\alpha_f,2}] [\mathbf{T}_{\alpha_i,1} \cdot \mathbf{T}_{\alpha_i,2}]}{(2\pi)^3} \int \frac{d^2 k_{2m\perp} dk_{2m}^+}{2(2\pi)^3 k_{2m}^+} \\
& {}_{1f} \langle \left( \Gamma_{\alpha_f} \frac{1}{2} \Gamma_{\alpha_i} \right) \rangle_{1m} \times {}_{2f} \langle \left( \Gamma_{\alpha_f} \frac{k_{2m}^+ + M}{2M} \Gamma_{\alpha_i} \right) \rangle_{2m} \\
& \theta(k_{2m}^+) \theta(k_{2i}^+ - k_{2m}^+) \theta(k_{2m}^+ - k_{2f}^+) \\
& \frac{F_{\alpha_f}(\mathbf{q}_f)^2}{(k_{2f}^+ - k_{2m}^+)(P^- - k_{1f}^- - k_{2m}^-) - m_{\alpha_f}^2 - (\mathbf{k}_{1f\perp} - \mathbf{k}_{1m\perp})^2} \frac{1}{2M} \\
& \frac{F_{\alpha_i}(\mathbf{q}_i)^2}{(k_{2i}^+ - k_{2m}^+)(P^- - k_{1i}^- - k_{2m}^-) - m_{\alpha_i}^2 - (\mathbf{k}_{1m\perp} - \mathbf{k}_{1i\perp})^2} \\
& + \{1 \leftrightarrow 2\}.
\end{aligned} \tag{68}$$

To get the contact potential for the pions, the following change has to be made:

$$[\mathbf{T}_{\alpha_f,1} \cdot \mathbf{T}_{\alpha_f,2}] [\mathbf{T}_{\alpha_i,1} \cdot \mathbf{T}_{\alpha_i,2}] \rightarrow \tau_2^2 = 3. \tag{69}$$

This is due the additional symmetry that the two pion vertex has.

Before this potential is used in calculations, it must be multiplied by a factor of  $\frac{M}{2(M+m_\pi)}$  (as discussed in section II E 1) if the crossed diagrams are not included.

## 7. Common Features and Simplification

Each of the potentials in Figs. 4 and 5 can be written schematically in the following general form:

$$\begin{aligned}
V_{\text{TME}} &= \frac{g^4 4M^2 T^4}{(2\pi)^3} \int \frac{d^2 k_{2m\perp} dk_{2m}^+}{2(2\pi)^3} f(k_{1m}^+, k_{2m}^+, q_f^+, q_i^+) \\
& {}_{1f} \langle \left( \Gamma_{\alpha_f} \mathcal{M}_1 \Gamma_{\alpha_i} \right) \rangle_{1m} \times {}_{2f} \langle \left( \Gamma_{\alpha_f} \mathcal{M}_2 \Gamma_{\alpha_i} \right) \rangle_{2m} \\
& [a_f - m_{\alpha_f}^2 + b_f \cos(\phi_f - \phi_m)]^{-n_f} F_{\alpha_f}(\mathbf{q}_f)^2 \\
& [a_m + b_{mf} \cos(\phi_f - \phi_m) + b_{mi} \cos(\phi_m - \phi_i)]^{-n_m} \\
& [a_i - m_{\alpha_i}^2 + b_i \cos(\phi_m - \phi_i)]^{-n_i} F_{\alpha_i}(\mathbf{q}_i)^2.
\end{aligned} \tag{70}$$

We use the expression for  $F_\alpha$  in Eq. (58) to get

$$\begin{aligned}
V_{\text{TME}} = & \frac{g^4 4M^2 T^4 (\Lambda^2 - m^2)^{4n_\alpha}}{(2\pi)^3} \int \frac{d^2 k_{2m\perp} dk_{2m}^+}{2(2\pi)^3} f(k_{1m}^+, k_{2m}^+, q_f^+, q_i^+) \\
& {}_{1f} \langle (\Gamma_{\alpha_f} \mathcal{M}_1 \Gamma_{\alpha_i}) \rangle_{1m} \times {}_{2f} \langle (\Gamma_{\alpha_f} \mathcal{M}_2 \Gamma_{\alpha_i}) \rangle_{2m} \\
& [a_f - m_{\alpha_f}^2 + b_f \cos(\phi_f - \phi_m)]^{-n_f} [a_f - \Lambda_{\alpha_f}^2 + b_f \cos(\phi_f - \phi_m)]^{-2n_{\alpha_f}} \\
& [a_m + b_{mf} \cos(\phi_f - \phi_m) + b_{mi} \cos(\phi_m - \phi_i)]^{-n_m} \\
& [a_i - m_{\alpha_i}^2 + b_i \cos(\phi_m - \phi_i)]^{-n_i} [a_i - \Lambda_{\alpha_i}^2 + b_i \cos(\phi_m - \phi_i)]^{-2n_{\alpha_i}}. \quad (71)
\end{aligned}$$

The TME potentials, like the OME potential, have exact rotational invariance about the  $z$ -axis, and thus conserve  $m$ . We project the potential onto states of definite  $m$  by setting  $\phi_i$  to zero and integrating the potential with  $\int d\phi_f e^{im\phi_f}/2\pi$ .

Now what we have to obtain the  $\bar{u}u$  matrix elements. In reference [46] shows that we can write

$$\begin{aligned}
& [{}_{1f} \langle (\Gamma_{\alpha_f} \mathcal{M}_1 \Gamma_{\alpha_i}) \rangle_{1m} \times {}_{2f} \langle (\Gamma_{\alpha_f} \mathcal{M}_2 \Gamma_{\alpha_i}) \rangle_{2m}]_{\phi_i=0} \\
& = \sum_{j,k} C_{j,k}(\Gamma_{\alpha_f}, \mathcal{M}_1, \Gamma_{\alpha_i}; \Gamma_{\alpha_f}, \mathcal{M}_2, \Gamma_{\alpha_i}) e^{ij(\phi_f - \phi_m)} e^{ik\phi_m}. \quad (72)
\end{aligned}$$

Note that the  $C$  is implicitly a function of the  $p_\perp$ ,  $p^+$ ,  $\phi$  and  $\lambda$  on both sides.

Then, after a change of variables,  $\phi_m \rightarrow \phi'_i$ ,  $\phi_f - \phi_m \rightarrow \phi'_f$ , and  $\phi_f \rightarrow \phi'_f + \phi'_i$ , the potential can be written as

$$\begin{aligned}
V_{\text{TME}} = & \frac{g^4 4M^2 T^4 (\Lambda^2 - m^2)^{4n_\alpha}}{(2\pi)^3} \sum_{j,k} \int \frac{dk_{2m\perp} k_{2m\perp} dk_{2m}^+}{2(2\pi)^2} f(k_{1m}^+, k_{2m}^+, q_f^+, q_i^+) \\
& C_{j,k}(\Gamma_{\alpha_f}, \mathcal{M}_1, \Gamma_{\alpha_i}; \Gamma_{\alpha_f}, \mathcal{M}_2, \Gamma_{\alpha_i}) \\
& \int_0^{2\pi} \frac{d\phi'_f}{2\pi} \int_0^{2\pi} \frac{d\phi'_i}{2\pi} e^{i(m+j)\phi'_f} e^{i(m+k)\phi'_i} \\
& [a_f - m_{\alpha_f}^2 + b_f \cos \phi'_f]^{-n_f} [a_f - \Lambda_{\alpha_f}^2 + b_f \cos \phi'_f]^{-2n_{\alpha_f}} \\
& [a_m + b_{mf} \cos \phi'_f + b_{mi} \cos \phi'_i]^{-n_m} \\
& [a_i - m_{\alpha_i}^2 + b_i \cos \phi'_i]^{-n_i} [a_i - \Lambda_{\alpha_i}^2 + b_i \cos \phi'_i]^{-2n_{\alpha_i}}. \quad (73)
\end{aligned}$$

The azimuthal-angle integrals taken together are denoted as  $I$ , and the method for calculating the  $\phi'_m$  and  $\phi'_f$  integrals is discussed in Ref. [46]. Summarizing, we can write

$$\begin{aligned}
V_{\text{TME}} = & \frac{g^4 4M^2 T^4 (\Lambda^2 - m^2)^{4n_\alpha}}{(2\pi)^3} \sum_{j,k} \int \frac{dk_{2m\perp} k_{2m\perp} dk_{2m}^+}{2(2\pi)^2} f(k_{1m}^+, k_{2m}^+, q_f^+, q_i^+) \\
& C_{j,k}(\Gamma_{\alpha_f}, \mathcal{M}_1, \Gamma_{\alpha_i}; \Gamma_{\alpha_f}, \mathcal{M}_2, \Gamma_{\alpha_i}) \\
& I(a_f - m_{\alpha_f}^2, a_f - \Lambda_{\alpha_f}^2, b_f, n_f, 2n_{\alpha_f}, m + j; \\
& \quad a_m, b_{mf}, b_{mi}, n_m; \\
& \quad a_i - m_{\alpha_i}^2, a_i - \Lambda_{\alpha_i}^2, b_i, n_i, 2n_{\alpha_i}, m + k). \quad (74)
\end{aligned}$$

This potential is evaluated using the numerical integration techniques discussed in Ref. [19].

### 8. Further Development of the Light-front Schrödinger Equation

The potentials derived here possess a high degree of symmetry. To solve the light-front Schrödinger equation efficiently, these symmetries should be explicitly exploited, as was done in Refs. [18, 19]. In addition to the invariance of the potentials under parity, there are additional symmetries due to the conservation of nucleon helicity and invariance under time reversal [22].

We follow Machleidt's approach for taking advantage of the symmetry of rotationally invariant potentials with helicity [23]. However, since the light-front potentials derived here do not have full rotational invariance, Machleidt's approach must be modified. The symmetry properties of helicity matrix elements are rederived in Ref. [46] without assuming full rotational invariance. These results allow a modified version of Machleidt's approach to be combined with the exploitation of parity (using the transformation from light-front coordinates to equal-time coordinates) discussed in Refs. [18, 19]. In particular, the potentials are initially calculated in the  $|p_{\text{ET}}, \theta, M, \lambda_1, \lambda_2\rangle$  basis, although the relations in Ref. [46] are used to transform to the  $|p_{\text{ET}}, J, M, L, S\rangle$  basis to solve for the wave functions. Note that the potentials connect states with different  $J$  values in general. Once the symmetries have been explicitly expressed, we can discretize the Schrödinger equation as done in Ref. [19].

Note that the transformations applied to the potential in order to simplify the solution of the wave functions. Once the wave functions are obtained, we may apply the inverse of the transformations to the wave functions to express them in the helicity basis ( $|\mathbf{p}_\perp, p^+, \lambda_1, \lambda_2\rangle$ ) or in the Bjorken and Drell spin basis ( $|\mathbf{p}_\perp, p^+, m_1, m_2\rangle$ ) [46].

## III. DEUTERON BINDING ENERGIES

The next step towards numerically calculating the bound states for these potentials is to choose the parameters (meson masses, coupling constants, etc.) for the potentials. We consider the full nuclear model where the nucleon-nucleon interaction is mediated by all the six mesons shown in Table I. For numerical work, use the parameters for the light-front nucleon-nucleon (LFNN) potential from the work of Miller and Machleidt [20]. Those parameters were fit for a potential that used a retarded propagator for the energy in the potentials. Since the potentials used in this paper have energy dependent denominators, the parameters must be modified somewhat. We choose to vary the coupling constant for the  $\sigma$  meson. The parameters are given in table I.

As with all the other deuteron models presented in this paper, the light-front one-meson-exchange (OME) potential breaks rotational invariance and causes a mass splitting of the deuteron states with different magnetic quantum numbers. We expect that the splitting will be removed somewhat by including higher order potentials.

The first step is to determine which two-meson-exchange potentials to use. One choice is to use only the two-pion-exchange potentials, TPE and ncTPE, as defined in the previous section. However, we expect to get better results using the two-meson-exchange diagrams generated by all the available mesons, including the contact diagrams for the pions, which we denote as the two-meson-exchange (TME) potential. In addition, we can also investigate the effect of leaving out the contact potentials for the pions, resulting in the non-chiral two-meson-exchange (ncTME) potential.

We do not include diagrams with a contact interaction between the nucleon, a pion, and another meson. This is because, as mentioned in section IIE1, the infinite series of

the box diagrams is rotationally invariant and the contact diagrams are not needed to achieve rotational invariance. Furthermore, they are not required to control the convergence of the series, since there is no strong cancellation between the contact diagram and the instantaneous diagrams.

The first step in analyzing the bound states is to determine what range of  $f_\sigma$  gives reasonable results. We iteratively solve for the binding energy of the deuteron, varying  $f_\sigma$  until the binding energy matches the physical value of the binding energy, for each of the potentials. The results are shown in Table II. We find that a value of  $f_\sigma$  in the range 1.2 to 1.3 will give reasonable results for the binding energy. Note that D-state probability (about 3%) is lower in this model than for the energy-independent light-front used in Ref. [20], where a value of 4.5% is found. This is expected since the  $f_\sigma$  is greater than 1 in this model, meaning that the scalar interaction is strengthened relative to the tensor interaction, leading to a decrease in amount of the D-state present.

We choose two values of  $f_\sigma$ , one from the low end of the range (1.22) and one from the high end (1.2815) for our investigations. Using two values helps ensure that our results are robust.

First, we examine the bound states for  $f_\sigma = 1.22$ . The results for several different choices of the TME potentials are shown in Table III and the binding energies are plotted in Fig. 6. In addition to the two-meson-exchange potentials mentioned above, we also consider the  $\pi$ - $\sigma$  plus  $\pi$ - $\omega$  Mesa potential. The reason for considering this potential is that Carbonell, Desplanques, Karmanov, and Mathiot [47] have shown that it helps restore rotational invariance of the deuteron.

In particular, they have used manifestly covariant light-front dynamics to analyze the deuteron. They start with a deuteron wave function calculated in equal-time dynamics, then use a light-front one-pion-exchange potential (expanded to lowest order in powers of  $\frac{1}{M}$ ) to calculate the perturbative corrections to the wave function. They find that the resulting wave function has an unphysical dependence on the orientation of the light-front plane, which would manifest itself as a breaking of rotational invariance in our formalism. They also use the  $\pi$ - $\sigma$  and  $\pi$ - $\omega$  Mesa potentials (expanded to lowest order in powers of  $\frac{1}{M}$ ) to calculate the correction to the wave function. When the wave function corrections are combined, they find that the directional dependence of the longest range part of the deuteron wave function cancels exactly.

This implies that for our model, using the  $\pi$ - $\sigma$  plus  $\pi$ - $\omega$  Mesa potential (which we denote by  $\pi$ -( $\sigma$ - $\omega$ )) should partially restore the rotational invariance of the deuteron, assuming that the breaking of rotational invariance is due primarily to the one-pion-exchange potential. Note that since we solve for the deuteron wave function self-consistently and to all orders for our potentials, we do not expect to find exactly the same result as Ref. [47].

The first thing to notice about the data in Table III is that the results are essentially the same regardless of if arbitrary angular momentum or is used or if the potential is restricted to the  $J = 1$  sector. The same result is also seen in the pion-only model [48]. It means that the wave functions are numerically approximate to angular momentum eigenstates.

Next we notice the splittings between masses and D state percentages for the  $m = 0$  and  $m = 1$  states. This implies that the states do not transform correctly under rotations. All of the two-meson-exchange potentials used reduce the splittings by similar amounts, by about 60% for the binding energy and by about 70% for the percent D state. Note also that the mass splittings for the pion-only model were much larger [48].

Examining the effects of the individual two-meson-exchange potentials, we see that  $\pi$ -( $\sigma$ -

$\omega$ ) potential does reduce the mass splitting, but it does not fully remove it. This is expected since the OME potential includes more than just the pion potential, and the potential is relativistic.

Next, we compare the ncTME and ncTPE potentials to the TME and TPE potentials. The non-chiral potentials reduce the binding energy more than the chiral potentials, as we expected from our experience from the pion-only model. However, unlike for the pion-only model, we find that the chiral and non-chiral potential have fairly similar effects [48].

Finally, notice that the mass splitting for the TPE potential is much smaller than for the other two-meson-exchange potentials. By itself, this does not imply that the rotational properties of the deuteron calculated with that potential are significantly better than those from other two-meson-exchange potentials. The individual potentials that make up the TME potential are fairly large in magnitude, but vary in sign. This means that using any subset of those potentials may result in either a larger or smaller mass splitting. In this case, it is smaller. To investigate this further, we examine the currents for the TME and TPE deuteron wave function in section IV.

To verify that our results are independent of the value of  $f_\sigma$ , we recalculate the deuteron properties for each of the potentials with  $f_\sigma = 1.2815$ . The results are summarized in Table IV, and the binding energies are shown in Fig. 7. The change in  $f_\sigma$  increases the binding of the states, but the rest of the results are qualitatively the same.

## IV. FORM FACTORS OF THE DEUTERON

In section III, we considered several different truncations of the light-front nucleon-nucleon (LFNN) potential and used them to obtain the deuteron wave function. In this section, we use those wave functions to solve for the matrix elements of the deuteron current operator, which is used to calculate the deuteron electromagnetic and axial form factors.

In this section, we first outline the covariant theory of the electromagnetic form factors for spin-1 objects, like the deuteron. Then we recall the features of light-front calculations (including the breaking of rotational invariance) of the form factors. After that, we review the covariant and light-front tools for calculating axial form factors. The formalism is then applied to calculate the electromagnetic and axial currents and form factors for the light-front deuteron wave functions.

### A. Electromagnetic Form Factors

#### 1. Covariant Theory

In the one-photon-exchange approximation, shown in Fig. 8, the amplitude of the scattering process  $ed \rightarrow ed$  is just the contraction of the electron and deuteron currents, multiplied by the photon propagator,

$$\langle p', \lambda' | j_\mu^e | p, \lambda \rangle \frac{1}{q^2} \langle k', m' | J_d^\mu | k, m \rangle, \quad (75)$$

where

$$\langle p', \lambda' | j_\mu^e | p, \lambda \rangle = e \bar{u}(p', \lambda') \gamma_\mu u(p, \lambda). \quad (76)$$

From Lorentz covariance, parity invariance, and time reversal invariance [49, 50, 51, 52, 53], we infer that the deuteron form factor can be written as

$$\langle k', m' | J_d^\mu | k, m \rangle = -\frac{e}{2M_d} (e^*)^\rho(\mathbf{k}', m') J_{\rho\sigma}^\mu e^\sigma(\mathbf{k}, m), \quad (77)$$

where the spin-1 polarization vectors satisfy

$$e_\mu^*(\mathbf{k}, m) e^\mu(\mathbf{k}, m') = -\delta_{m, m'}, \quad (78)$$

$$\sum_m e_\mu^*(\mathbf{k}, m) e_\nu(\mathbf{k}, m) = -g_{\mu\nu} + \frac{k_\mu k_\nu}{M_d^2}, \quad (79)$$

$$k_\mu e^\mu(\mathbf{k}, m) = 0, \quad (80)$$

and the operator  $J_{\rho\sigma}^\mu$  is given by

$$J_{\rho\sigma}^\mu = (k'_\mu + k_\mu) \left[ g_{\rho\sigma} F_1(q^2) - \frac{q_\rho q_\sigma}{2M_d^2} F_2(q^2) \right] - I_{\rho\sigma}^{\mu\nu} q_\nu G_1(q^2), \quad (81)$$

where  $I_{\rho\sigma}^{\mu\nu} = g_\rho^\mu g_\sigma^\nu - g_\rho^\nu g_\sigma^\mu$  is the generator of infinitesimal Lorentz transformations,  $q = k' - k$ , and  $F_1$ ,  $F_2$ , and  $G_1$  are functions of  $q^2$ , the invariant mass of the photon. Some conventions [10, 17] denote  $G_1$  as  $-F_3$ .

The  $F_1$ ,  $F_2$ , and  $G_1$  form factors are related to the deuteron charge, magnetic, and quadrupole form factors, denoted by  $F_C$ ,  $F_M$ , and  $F_Q$  respectively, by [49, 51, 54]

$$F_C = F_1 + \frac{2}{3}\eta [F_1 + (1 + \eta)F_2 - G_1], \quad (82)$$

$$F_M = G_1, \quad (83)$$

$$F_Q = F_1 + (1 + \eta)F_2 - G_1, \quad (84)$$

where

$$\eta = \frac{-q^2}{4M_d^2}. \quad (85)$$

Note that since both the initial and final electron and deuteron are on-shell,  $-q^2 > 0$ . We define  $Q^2 = -q^2$ .

At zero-momentum transfer, the deuteron charge, magnetic, and quadrupole form factors are simply

$$F_C(0) = 1, \quad (86)$$

$$F_M(0) = \frac{M_d}{m_p} \mu_d = 1.71293, \quad (87)$$

$$F_Q(0) = M_d^2 Q_d = 25.8525, \quad (88)$$

where  $m_p$  is the mass of the proton,  $\mu_d$  is the magnetic moment of the deuteron (in nuclear magnetons  $\mu_N = \frac{e}{2m_p}$ ), and  $Q_d$  is the electric quadrupole moment of the deuteron (in units of the deuteron mass, although typically it is measured in  $e$ -barns). The numerical values of the form factors are determined by using experimentally measured values [52, 55, 56].

Another set of form factors are  $G_0$ ,  $G_1$ , and  $G_2$ , commonly used in light-front dynamics [10, 13, 17]. They are simply related to the charge, magnetic, and quadrupole form factors,

$$G_0 = F_C, \quad (89)$$

$$G_1 = -F_M, \quad (90)$$

$$G_2 = \frac{\sqrt{8}}{3}\eta F_Q. \quad (91)$$

The electron-deuteron cross-section is measured to determine the deuteron form factors for large momentum transfers. The unpolarized cross-section has the form [52, 57]

$$\frac{d\sigma}{d\Omega_e} = \frac{\sigma_{\text{Mott}}}{1 + \frac{2E_e}{M_d} \sin^2 \frac{\theta_e}{2}} \left( A(Q^2) + B(Q^2) \tan^2 \left( \frac{\theta_e}{2} \right) \right), \quad (92)$$

where

$$\sigma_{\text{Mott}} = \left( \frac{\alpha \cos \frac{\theta_e}{2}}{2E_e \sin^2 \frac{\theta_e}{2}} \right)^2, \quad (93)$$

and  $E_e$  is the electron beam energy,  $\theta_e$  is the angle by which the electron scatters, and  $\alpha$  is the fine-structure constant. The structure functions  $A$  and  $B$  can be expressed in terms of the charge, magnetic, and quadrupole form factors,

$$A = F_c^2 + \frac{8}{9}\eta^2 F_Q^2 + \frac{2}{3}\eta F_M^2, \quad (94)$$

$$B = \frac{4}{3}\eta(1 + \eta)F_M^2. \quad (95)$$

The three form factors  $F_1$ ,  $F_2$ , and  $G_1$  cannot be determined uniquely from the unpolarized scattering data since that measurement provides only two structure functions. More information is needed, which can be obtained from experiments where the polarization of the electron and/or deuteron is measured [52, 53]. The most commonly measured quantity is the tensor polarization observable,  $T_{20}$ ,

$$T_{20} = -\frac{\frac{8}{3}\eta F_C F_Q + \frac{8}{9}\eta^2 F_Q^2 + \frac{1}{3}\eta F_M^2 \left( 1 + 2(1 + \eta) \tan^2 \frac{\theta_e}{2} \right)}{\sqrt{2} \left( A + B \tan^2 \frac{\theta_e}{2} \right)}. \quad (96)$$

Note that  $T_{20}$  depends on the angle  $\theta_e$ . For ease of comparison, data for  $T_{20}$  is usually presented for  $\theta_e = 70^\circ$ . Alternatively, one can eliminate the angular dependence by defining  $\tilde{T}_{20}$ , which is  $T_{20}$  with  $F_M$  set equal to zero,

$$\tilde{T}_{20} = -\frac{\frac{8}{3}\eta F_C F_Q + \frac{8}{9}\eta^2 F_Q^2}{\sqrt{2} \left( F_C^2 + \frac{8}{9}\eta^2 F_Q^2 \right)}. \quad (97)$$

The extraction of the structure functions from the data is difficult. In practice, each cross-section measurement is performed at a different momentum transfer and angle, making it impossible to exactly disambiguate, for example,  $A$  and  $B$ . One needs to interpolate between values of  $B$  to calculate values for  $A$ , and vice versa. The Jefferson Lab  $t_{20}$  Collaboration used a self-consistent method for obtaining the structure functions from the scattering data [58]. They consider a variety of theoretical models for the deuteron form factors, then fit the parameters of the models to the measured cross-sections. After each model is fit, it is used as the interpolation function to disentangle the structure functions. This two-step process helps minimize model-dependent effects in the values of  $A$  and  $B$ .

## 2. Light Front Calculation

Light-front dynamics is particularly well suited to calculating form factors. One reason is that the generators of boosts in the one, two, and plus directions are kinematic, so that wave functions calculated with a truncated potential transform correctly under boosts. This feature is especially important for form factors at high momentum transfer since the wave functions must undergo a large boost.

Another, more subtle, reason for using the light front is that many of the graphs which contribute to the current vanish identically. For example, the three lowest-order graphs for the current are shown in Fig. 9. The double line denotes the deuteron, and the vertex of the deuteron lines and the nucleon lines represents the deuteron wave function. The graph labeled (a) does not vanish and is calculated in section IV A 5.

Fig. 9(b) vanishes in light-front dynamics. To see why, we first note three facts: the plus component of each particle in light-front dynamics is non-negative (for massive particles it must be positive), the plus component of the momentum is conserved, and the plus momentum of the vacuum is zero. Combining these facts, we find that any vertex which has particles on one side and vacuum on the other must vanish. In other words, the vacuum is trivially empty, and no graphs couple to it.

For Fig. 9(c), the coupling of the photon to the nucleon goes like  $\bar{u}_{\text{LF}}\gamma^\mu v_{\text{LF}}$ , where the light-front spinors are defined in the Appendix. For  $\mu = +$ , this matrix element is suppressed maximally, and thus  $J^+$  is the “good” component of the current [10, 12, 59]. We calculate only  $J^+$ , since it is the most stable.

We do not consider the contribution of higher-order graphs to the deuteron current, such as graphs where the photon couples to a meson or a nucleon while a meson is present. The omission of the meson-exchange currents does not affect the rotational properties of the current, although it does affect the overall values of the deuteron form factors. This is acceptable since we are only concerned with the rotational properties in this work, not in the detailed results.

The neglect of the graphs where the photon couples to a nucleon while a meson is present may affect the rotational properties of the current. This is because the deuteron current shown in Fig. 9(a) is not formally conserved [57], but current conservation is necessary (although not sufficient) for the current to have the correct properties under rotation. To construct the conserved current operator associated with a given wave function, the current must include diagrams that are related to the potential used to calculate the wave function. We expect that these diagrams are small since they contain meson propagators, and that neglecting them should not significantly affect the conservation of the deuteron current or the rotational properties of the current.

## 3. Symmetries of the Electromagnetic Current

Now, we use symmetries to relate the components of  $\langle k', m' | J^+(q) | k, m \rangle$ . Although in light-front dynamics some generators of Lorentz transformations are dynamic, such as the generators of rotations from the  $x$ - $y$  plane into the  $x$  direction are dynamic, we are free to boost in the plane perpendicular to the  $z$ -axis, boost in the plus direction, and rotate about the  $z$ -axis, since the generators of those transformations are kinematic. In addition, we will find how the states and the current operator transforms under parity and time-reversal.

The kinematic generators allow us to choose which frame to evaluate the current in. We



choose the Breit frame [10], where  $q^+ = q^- = q_\perp^y = 0$  and  $q_\perp^x = Q$ . We also choose the plus momentum of the deuteron to be  $M_d$ , since  $M_d$  is value of the plus momentum in deuteron's rest frame. To simplify notation, we define the matrix elements of  $J^+$  as

$$I_{m',m}^+(Q) = \left\langle \frac{\mathbf{q}_\perp}{2}, m' \left| J^+(Q) \right| -\frac{\mathbf{q}_\perp}{2}, m \right\rangle. \quad (98)$$

This quantity is represented with  $I_{m'm}$  instead of  $J_{m'm}$  because  $J_{m'm}$  is used to represent the matrix elements of  $J$  using the instant-form spin basis. This distinction is discussed later in this section.

Next, we consider rotation about the  $z$ -axis by  $\pi$  ( $R_z(\pi)$ ), parity ( $\Pi$ ), and time-reversal ( $\Theta$ ). First note that the current operator transforms as

$$R_z(\pi)J^\pm R_z(\pi) = J^\pm, \quad (99)$$

$$\Pi J^\pm \Pi = J^\mp, \quad (100)$$

$$\Theta J^\pm \Theta = J^\mp. \quad (101)$$

Obviously, we must use both parity and time reversal to retain the plus component of the current. Now look at how the deuteron states transform:

$$R_z(\pi)|-\mathbf{k}_\perp, m\rangle = |+\mathbf{k}_\perp, m\rangle(-1)^m, \quad (102)$$

$$\Theta\Pi|-\mathbf{k}_\perp, m\rangle = |-\mathbf{k}_\perp, -m\rangle(-1)^m. \quad (103)$$

Although the symmetry operators can introduce extra, constant phase factors, they are omitted here since they cancel when calculating matrix elements. These results make it easy to find what each of these symmetry operators does to the matrix element. Under rotations a rotation of  $\pi$  about the  $z$ -axis, the current matrix element transforms to

$$I_{m',m}^+(Q) \rightarrow (-1)^{m-m'} \left\langle -\frac{\mathbf{q}_\perp}{2}, m' \left| J^+(Q) \right| +\frac{\mathbf{q}_\perp}{2}, m \right\rangle. \quad (104)$$

Under parity followed by time reversal, the matrix element becomes

$$I_{m',m}^+(Q) \rightarrow (-1)^{m-m'} \left\langle -\frac{\mathbf{q}_\perp}{2}, -m \left| J^+(Q) \right| +\frac{\mathbf{q}_\perp}{2}, -m' \right\rangle. \quad (105)$$

$$(106)$$

Since  $J^\mu$  is Hermitian, we can also take the complex conjugate of the matrix element to get

$$I_{m',m}^+(Q) \rightarrow \left\langle -\frac{\mathbf{q}_\perp}{2}, m \left| J^+(Q) \right| +\frac{\mathbf{q}_\perp}{2}, m' \right\rangle. \quad (107)$$

The appropriate combinations of Eqs. (104-107) give [17]

$$I_{m',m}^+(Q) = (-1)^{m-m'} I_{-m',-m}^+(Q), \quad (108)$$

$$= (-1)^{m-m'} I_{m,m'}^+(Q). \quad (109)$$

The same relations also apply for  $J_{m'm}^+$  matrix elements. Eqs. (108) and (109) imply that of the nine possible matrix elements of  $J^+$ , there are only four independent components. We choose those components to be  $I_{11}^+$ ,  $I_{10}^+$ ,  $I_{1-1}^+$ , and  $I_{00}^+$ . It is helpful to express the matrix elements in a matrix to see the symmetry properties explicitly.

$$I_{m',m}^+ = \begin{pmatrix} I_{11}^+ & I_{10}^+ & I_{1-1}^+ \\ -I_{10}^+ & I_{00}^+ & I_{10}^+ \\ I_{1-1}^+ & -I_{10}^+ & I_{11}^+ \end{pmatrix}. \quad (110)$$

#### 4. Rotational Invariance and the Angular Condition

This is as far as we can go with light-front dynamics, but there should be an additional redundancy in our matrix elements. We have derived four independent components, whereas in a fully covariant framework there are only three form factors. The resolution of this conflict is that full rotational invariance imposes an *angular condition* on the light-front matrix elements.

The angular condition can be found by using the deuteron polarization vectors for the Breit frame to calculate the current given in Eq. (77) in terms of  $F_1$ ,  $F_2$ , and  $G_1$ . By comparing that result with Eq. (110), we obtain linear relations between the current matrix elements ( $I_{11}^+$ ,  $I_{10}^+$ ,  $I_{1-1}^+$ , and  $I_{00}^+$ ) and the form factors ( $F_1$ ,  $F_2$ , and  $G_1$ ) and also find that in general there is a deviation from the angular condition, which we denote with  $\Delta$ , given by [13]

$$\Delta = -I_{00}^+ + (1 + 2\eta)I_{11}^+ + I_{1-1}^+ - 2\sqrt{2\eta}I_{10}^+, \quad (111)$$

where  $\eta$  is defined by Eq. (85). Since  $\Delta$  vanishes when the deuteron current transforms correctly under rotations, we interpret  $\Delta$  as a measure of the extent to which the current transforms incorrectly.

The form factors are overdetermined by the current matrix elements, which means there are many different relations between them are possible. When  $\Delta$  is zero, the angular condition can be used to show that all the relations are equivalent, while a non-zero  $\Delta$  means that the form factors depend also on which relation is chosen.

Since  $\Delta$  is non-zero in general, it is important to choose the best relation to obtain the form factor. To do this, we classify the current matrix elements as either “good” or “bad”. This classification is similar to the one made for choosing which component of the current to use.

In this work we are interested in the overall rotational invariance properties; the choice of how to relate the form factors is simply useful for comparing with other approaches. In that spirit, we consider four different choices [13]. First, Grach and Kondratyuk (GK) derive a relation in which  $I_{00}^+$  is considered bad. Using the angular condition to eliminate the  $I_{00}^+$  for the equations, they obtain [60]

$$G_{0,GK} = \frac{1}{3} \left[ (3 - 2\eta)I_{11}^+ + 2\sqrt{2\eta}I_{10}^+ + I_{1-1}^+ \right], \quad (112)$$

$$G_{1,GK} = 2 \left( I_{11}^+ - \frac{1}{\sqrt{2\eta}}I_{10}^+ \right), \quad (113)$$

$$G_{2,GK} = \frac{2\sqrt{2}}{3} \left( -\eta I_{11}^+ + \frac{2\eta^+}{I_{10}} - I_{1-1}^+ \right). \quad (114)$$

Brodsky and Hiller (BH) use a prescription where  $I_{11}^+$  is bad, which results in [61]

$$G_{0,BH} = \frac{1}{3(1 + 2\eta)} \left[ (3 - 2\eta)I_{00}^+ + 8\sqrt{2\eta}I_{10}^+ + 2(2\eta - 1)I_{1-1}^+ \right], \quad (115)$$

$$G_{1,BH} = \frac{2}{1 + 2\eta} \left[ I_{00}^+ - I_{1-1}^+ + (2\eta - 1) \frac{I_{10}^+}{\sqrt{2\eta}} \right], \quad (116)$$

$$G_{2,BH} = \frac{2\sqrt{2}}{3(1 + 2\eta)} \left[ \sqrt{2\eta}I_{10}^+ - \eta I_{00}^+ - (1 + \eta)I_{1-1}^+ \right]. \quad (117)$$

Frankfurt, Frederico, and Strikman (FFS) start by analyzing the deuteron current using an equal-time spin basis, where the current matrix elements are  $J_{m'm}^+$  [10]. Their prescription uses the Cartesian basis to find that  $J_{zz}^+$  is the bad current. Upon transformation to the spherical basis and use of the Melosh transformation [12, 62] to relate  $J_{m'm}^+$  to  $I_{m'm}^+$ , they find

$$G_{0,FFS} = \frac{1}{3(1+\eta)} \left[ (2\eta+3)I_{11}^+ + 2\sqrt{2\eta}I_{10}^+ - \eta I_{00}^+ + (2\eta+1)I_{1-1}^+ \right], \quad (118)$$

$$G_{1,FFS} = \frac{1}{1+\eta} \left[ I_{11}^+ + I_{00}^+ - I_{1-1}^+ - \frac{2(1-\eta)}{\sqrt{2\eta}} I_{10}^+ \right], \quad (119)$$

$$G_{2,FFS} = \frac{\sqrt{2}}{3(1+\eta)} \left[ -\eta I_{11}^+ + 2\sqrt{2\eta}I_{10}^+ - \eta I_{00}^+ - (\eta+2)I_{1-1}^+ \right]. \quad (120)$$

Chung, Polyzou, Coester, and Keister (CCKP) choose the canonical expressions for the form factors  $G_0$ ,  $G_1$ , and  $G_2$  in terms of the equal-time current as the starting point [17, 54]. They use rotations and the Melosh transformation to express the equal-time current matrix elements in terms of the light-front current matrix elements, and find that

$$G_{0,CCKP} = \frac{1}{6(1+\eta)} \left[ (3-2\eta)(I_{11}^+ + I_{00}^+) + 10\sqrt{2\eta}I_{10}^+ + (4\eta-1)I_{1-1}^+ \right], \quad (121)$$

$$G_{1,CCKP} = G_{1,FFS}, \quad (122)$$

$$G_{2,CCKP} = G_{2,FFS}. \quad (123)$$

### 5. Impulse Approximation on the Light Front

We now are ready to relate the deuteron wave function to the current expressed in Eq. (98). The deuteron wave functions solved in section II are used. We use the representation of the wave function in the spin  $|\mathbf{p}_\perp, p^+, m_1, m_2\rangle$  basis, as discussed in Sec. II E 8. Note that these spins are expressed in the usual Bjorken and Drell representation [63]. By inserting a complete set of states into Eq. (98) and making the momentum of particle 1 explicit, we get

$$\begin{aligned} J_{m',m}^+(q) = & \int d^2p_\perp dp^+ \sum_{m'_1, m_1, m_2} \left\langle \frac{\mathbf{q}_\perp}{2}, m' \left| p^+, \mathbf{p}_\perp + \frac{\mathbf{q}_\perp}{2}, m'_1, m_2 \right\rangle \right. \\ & 2 \left\langle p^+, \mathbf{p}_\perp + \frac{\mathbf{q}_\perp}{2}, m'_1 \left| J_{(S)}^+(\mathbf{q}_\perp) \right| p^+, \mathbf{p}_\perp - \frac{\mathbf{q}_\perp}{2}, m_1 \right\rangle \\ & \left. \left\langle p^+, \mathbf{p}_\perp - \frac{\mathbf{q}_\perp}{2}, m_1, m_2 \left| -\frac{\mathbf{q}_\perp}{2}, m \right\rangle, \right. \end{aligned} \quad (124)$$

where the spin directions of particles 1 and 2 are labeled  $m_1$  and  $m_2$ , respectively. Also, since the deuteron is an isoscalar combination of nucleons, the isovector component of the nucleon current does not contribute and the isoscalar nucleon current is the same for both nucleons. This allows us to simply double the isoscalar current of particle 1 instead of using the isoscalar currents of both particle 1 and 2.

We want to boost the deuteron wave functions to the rest frame, since that is where the wave functions are calculated. Note that the boosts in the  $x$ - $y$  plane transforms a general

vector  $(\mathbf{k}_\perp, k^+)$  by  $\mathbf{k}_\perp \rightarrow \mathbf{k}_\perp - \mathbf{q}_\perp \frac{k^+}{q^+}$ , leaving  $k^+$  unchanged. This means that the boost that puts the deuteron in its rest frame transforms the individual nucleon momentum by

$$\mathbf{p}_\perp - \frac{\mathbf{q}_\perp}{2} \rightarrow \mathbf{p}_\perp - (1-x) \frac{\mathbf{q}_\perp}{2}, \quad (125)$$

where we use the Bjorken  $x$ -variable  $x = \frac{p^+}{M_d}$ . Note that the spin labels do not change. This is because the boost is in the perpendicular direction, so the spin labels (defined to point in the  $z$  direction) are not affected.

This allows Eq. (124) to be written as [14]

$$\begin{aligned} J_{m',m}^+(q) &= \int d^2 p_\perp dp^+ \sum_{m'_1, m_1, m_2} \left\langle m' \left| p^+, \mathbf{p}_\perp + (1-x) \frac{\mathbf{q}_\perp}{2}, m'_1, m_2 \right\rangle \right. \\ &\quad 2 \left\langle p^+, \mathbf{p}_\perp + \frac{\mathbf{q}_\perp}{2}, m'_1 \left| J_{(S)}^+(\mathbf{q}_\perp) \right| p^+, \mathbf{p}_\perp - \frac{\mathbf{q}_\perp}{2}, m_1 \right\rangle \\ &\quad \left. \left\langle p^+, \mathbf{p}_\perp - (1-x) \frac{\mathbf{q}_\perp}{2}, m_1, m_2 \left| m \right\rangle \right. \right). \end{aligned} \quad (126)$$

We have dropped explicit mention of the deuteron's momentum.

Before we continue, we note that we can write the nucleon current matrix elements using the  $u$  spinors,

$$\begin{aligned} &\left\langle p^+, \mathbf{p}_\perp + \frac{\mathbf{q}_\perp}{2}, m'_1 \left| J_{(S)}^+(\mathbf{q}_\perp) \right| p^+, \mathbf{p}_\perp - \frac{\mathbf{q}_\perp}{2}, m_1 \right\rangle \\ &= \bar{u}_{\text{BD}} \left( p^+, \mathbf{p}_\perp + \frac{\mathbf{q}_\perp}{2}, m'_1 \right) J_{(S)}^+(\mathbf{q}_\perp) u_{\text{BD}} \left( p^+, \mathbf{p}_\perp - \frac{\mathbf{q}_\perp}{2}, m_1 \right), \end{aligned} \quad (127)$$

where we have used the ‘‘BD’’ subscript to denote these as Bjorken and Drell spinors. Since the nucleons are on-shell, as they must be in a Hamiltonian theory, we interpret  $u_{\text{BD}}(p^+, \mathbf{p}_\perp, m)$  as  $u_{\text{BD}}(p_x = p_{\perp,x}, p_y = p_{\perp,y}, p_z = \frac{p^+ - p^-}{2})$ , where  $p^- = \frac{M^2 + p_\perp^2}{p^+}$ .

However, the matrix elements can be calculated easily if we convert the Bjorken and Drell spinors to light-front spinors. This transformation is formally accomplished with the Melosh transformation  $R_M$ , given by [10, 17],

$$R_M = \frac{p^+ + M - i\boldsymbol{\sigma} \cdot (\mathbf{n} \times \mathbf{p}_\perp)}{\sqrt{(p^+ + M)^2 + p_\perp^2}}, \quad (128)$$

where  $\mathbf{n}$  points in the direction of the light front. Note that the Melosh transformation is unitary.

This transformation converts a Bjorken and Drell spinor to a light-front spinor in the following manner,

$$u_{\text{LF}}(p^+, \mathbf{p}_\perp, m) = \sum_{m'} (R_M^\dagger)_{m,m'} u_{\text{BD}}(p^+, \mathbf{p}_\perp, m'). \quad (129)$$

Using this transformation, we rewrite Eq. (126) as

$$\begin{aligned} J_{m',m}^+(q) &= \int d^2 p_\perp dp^+ \sum_{m'_1, m_1, m_2} \left[ \sum_{m''_1} \left\langle m' \left| p^+, \mathbf{p}_\perp + (1-x) \frac{\mathbf{q}_\perp}{2}, m''_1, m_2 \right\rangle (R_M)_{m''_1, m'_1} \right] \\ &\quad 2\bar{u}_{\text{LF}} \left( p^+, \mathbf{p}_\perp + \frac{\mathbf{q}_\perp}{2}, m'_1 \right) J_{(S)}^+(\mathbf{q}_\perp) u_{\text{LF}} \left( p^+, \mathbf{p}_\perp - \frac{\mathbf{q}_\perp}{2}, m_1 \right) \\ &\quad \left[ \sum_{m'''_1} (R_M^\dagger)_{m'''_1, m_1} \left\langle p^+, \mathbf{p}_\perp - (1-x) \frac{\mathbf{q}_\perp}{2}, m'''_1, m_2 \left| m \right\rangle \right]. \end{aligned} \quad (130)$$

## 6. The Nucleon Form Factors

From Lorentz covariance, parity invariance, and time reversal invariance [50, 51], the isoscalar part of the nucleon current can be expressed as

$$J_{(S)}^\mu(q) = \gamma^\mu F_1^{(S)}(q) + i \frac{\sigma^{\mu\nu} q_\nu}{2M} F_2^{(S)}(q). \quad (131)$$

Taking the matrix elements of  $J^+$  with the light-front spinors gives

$$\begin{aligned} \bar{u}(k', \lambda') J_{(S)}^+(q_\perp) u(k, \lambda) &= F_1^{(S)}(q) \bar{u}_{\text{LF}}(k', \lambda') \gamma^+ u_{\text{LF}}(k, \lambda) \\ &\quad + F_2^{(S)}(q) \frac{q_\perp^i}{2M} \bar{u}_{\text{LF}}(k', \lambda') \gamma^+ \gamma_\perp^i u_{\text{LF}}(k, \lambda), \end{aligned} \quad (132)$$

where we have parameterized

$$k'^+ = k^+, \quad (133)$$

$$\mathbf{k}_\perp = \mathbf{p}_\perp + \frac{\mathbf{q}_\perp}{2}, \quad (134)$$

$$\mathbf{k}'_\perp = \mathbf{p}_\perp - \frac{\mathbf{q}_\perp}{2}. \quad (135)$$

We use the representation of the spinors given in the Appendix to simplify the spinor matrix elements appearing in Eq. 132. First consider

$$\begin{aligned} \bar{u}_{\text{LF}}(k', \lambda') \gamma^+ u_{\text{LF}}(k, \lambda) &= \frac{1}{M k^+} \chi_{\text{LF}, \lambda'}^\dagger \left[ (M - \boldsymbol{\alpha}^\perp \cdot \mathbf{k}'^\perp) \Lambda_+ + k^+ \Lambda_- \right] \gamma^+ \\ &\quad \times \left[ \Lambda_- (M + \boldsymbol{\alpha}^\perp \cdot \mathbf{k}^\perp) + \Lambda_+ k^+ \right] \chi_{\text{LF}, \lambda}, \end{aligned} \quad (136)$$

$$= \frac{k^+}{M} \delta_{\lambda' \lambda}. \quad (137)$$

Next,

$$\begin{aligned} \bar{u}_{\text{LF}}(k', \lambda') \gamma^+ \gamma_\perp^i u_{\text{LF}}(k, \lambda) &= \frac{1}{M k^+} \chi_{\text{LF}, \lambda'}^\dagger \left[ (M - \boldsymbol{\alpha}^\perp \cdot \mathbf{k}'^\perp) \Lambda_+ + k^+ \Lambda_- \right] \gamma^+ \gamma^i \\ &\quad \times \left[ \Lambda_- (M + \boldsymbol{\alpha}^\perp \cdot \mathbf{k}^\perp) + \Lambda_+ k^+ \right] \chi_{\text{LF}, \lambda}, \end{aligned} \quad (138)$$

$$= \frac{k^+}{M} \chi_{\text{LF}, \lambda'}^\dagger \gamma^+ \gamma_\perp^i \chi_{\text{LF}, \lambda}, \quad (139)$$

$$= -i \epsilon^{ij3} \frac{k^+}{M} \chi_{\lambda'}^\dagger \sigma^j \chi_\lambda. \quad (140)$$

Combining these, we find [10, 12]

$$\langle k', \lambda' | J_{(S)}^+(q_\perp) | k, \lambda \rangle = \frac{k^+}{M} \chi_{\lambda'}^\dagger \left[ F_1^{(S)}(q) - \frac{1}{2M} F_2^{(S)}(q) \left( i q_\perp^i \epsilon^{ij3} \sigma_\perp^j \right) \right] \chi_\lambda \quad (141)$$

We can rewrite Eq. (141) as

$$\begin{aligned} \langle k', \lambda' | J_{(S)}^+(q_\perp) | k, \lambda \rangle &= F_1^{(S)}(q) \langle k', \lambda' | J_{(1S)}^+(q_\perp) | k, \lambda \rangle + \\ &\quad F_2^{(S)}(q) \langle k', \lambda' | J_{(2S)}^+(q_\perp) | k, \lambda \rangle, \end{aligned} \quad (142)$$

which, when inserted into Eq. (130), gives

$$I_{m',m}^+(q) = F_1^{(S)}(q)I_{(1)m',m}^+(q) + F_2^{(S)}(q)I_{(2)m',m}^+(q), \quad (143)$$

where we define

$$\begin{aligned} I_{(i)m',m}^+(q) = & \int d^2p_\perp dp^+ \sum_{m'_1, m_1, m_2} \langle m' | p^+, \mathbf{p}_\perp + (1-x)\frac{\mathbf{q}_\perp}{2}, m'_1, m_2 \rangle \\ & 2 \langle p^+, \mathbf{p}_\perp + \frac{\mathbf{q}_\perp}{2}, m'_1 | J_{(iS)}^+(\mathbf{q}_\perp) | p^+, \mathbf{p}_\perp - \frac{\mathbf{q}_\perp}{2}, m_1 \rangle \\ & \langle p^+, \mathbf{p}_\perp - (1-x)\frac{\mathbf{q}_\perp}{2}, m_1, m_2 | m \rangle, \end{aligned} \quad (144)$$

for  $i = 1, 2$ . Note that both  $J_{(1)m',m}^+(q)$  and  $J_{(2)m',m}^+(q)$  must satisfy the same equations as  $J_{m',m}^+(q)$  does. In particular, this means that the angular condition should apply to  $J_{(1)m',m}^+(q)$  and  $J_{(2)m',m}^+(q)$  independently, so we consider the deviation from the angular condition for each.

There are many parameterizations of the isoscalar nucleon form factors  $F_1^{(S)}(q)$  and  $F_2^{(S)}(q)$ . Since the measurement of the electron-nucleon cross section is difficult, the data have large errors and are consistent with several different models of the nucleon form factors. Some of the models representative of those proposed in the literature are: the dipole model, fit 8.2 of Hohler [64], Gari:1985 [65], model 3 of Gari:1992 [66, 67], best fit for the multiplicative parameterization of Mergell [68], and model DR-GK(1) of Lomon [69]. The  $F_1^{(S)}(q)$  and  $F_2^{(S)}(q)$  form factors for each of these models are shown in Fig. 10.

We can relate the isovector form factors to  $G_{Ep}$ ,  $G_{Mp}$ ,  $G_{En}$ , and  $G_{Mn}$ , the proton electric, proton magnetic, neutron electric, and neutron magnetic form factors, respectively, with [70]

$$F_1^{(S)} = \frac{G_{Ep} + G_{En} + \tau(G_{Mp} + G_{Mn})}{2(1 + \tau)}, \quad (145)$$

$$F_2^{(S)} = \frac{-G_{Ep} - G_{En} + G_{Mp} + G_{Mn}}{2(1 + \tau)}, \quad (146)$$

where  $\tau \equiv \frac{Q^2}{4M}$ . The value of  $\tau$  is approximately 1 at a momentum transfer of about 5 GeV<sup>2</sup>, the upper range of momentum transfers that we consider. Since the overall magnitudes of the form factors are similar at this momentum transfer, it is important to measure each of the form factors with the same accuracy and cover the same range of momentum transfers. Currently, the most poorly known form factor is  $G_{En}$ , both in terms of the magnitude of the error and in the number of data points [69].

In section V, we will find that for momentum transfers greater than about 2 GeV<sup>2</sup>, the spread in the values of the deuteron form factors due to the breaking of rotational invariance on the light front is smaller than the spread in values due to using the various nucleon form factors. It is uncertainty of the nucleon form factors, not the use of the light front, that limits the accuracy of the deuteron form factors at large momentum transfers. Only more accurate measurements of the nucleon form factors, especially  $G_{En}$ , will allow for more accurate deuteron form factor calculations.

## B. Axial Form Factors

The formalism used for the axial current and form factor is very similar to that used for the electromagnetic current and form factor. Thus, most of the discussion from the previous

section carries over here with only slight modifications. We highlight only the differences.

The derivation of the symmetries of the axial current matrix elements is almost the same as in section IV A 2, with the exception that under parity, the axial current picks up a negative sign

$$\Pi J_5^\pm \Pi = -J_5^\mp. \quad (147)$$

When this is propagated through the algebra, we find that

$$I_{(5)m',m}^+(Q) = -(-1)^{m-m'} I_{(5)-m',-m}^+(Q), \quad (148)$$

$$= (-1)^{m-m'} I_{(5)m,m'}^+(Q). \quad (149)$$

Eqs. (148) and (149) imply that of the nine possible matrix elements of  $J_5^+$ , there are only two independent components. We choose those components to be  $I_{(5)11}^+$ , and  $I_{(5)10}^+$ . It is helpful to express the matrix elements in a matrix to see the symmetry properties explicitly.

$$I_{(5)m',m}^+ = \begin{pmatrix} I_{(5)11}^+ & I_{(5)10}^+ & 0 \\ -I_{(5)10}^+ & 0 & -I_{(5)10}^+ \\ 0 & I_{(5)10}^+ & -I_{(5)11}^+ \end{pmatrix}. \quad (150)$$

We have derived two independent components, but an analysis of the covariant theory shows that only one deuteron form factor ( $F_A$ ) contributes for the plus component of the axial current [11]. This implies that the requirement of full rotational invariance imposes an angular condition on the light-front axial current matrix elements. The deviation from the angular condition, denoted by  $\Delta$ , given by [11],

$$\Delta = \frac{\sqrt{2\eta}}{2} I_{(5)11}^+ - I_{(5)10}^+. \quad (151)$$

Since the deuteron axial form factor is overdetermined by the current matrix elements, we need to classify the current matrix elements as either “good” or “bad” to eliminate ambiguity. We consider two such choices.

Frankfurt, Frederico, and Strikman (FFS) find that the  $J_{(5)zz}^+$  is the bad matrix element [10]. After transforming to the spherical basis and using the Melosh transformation, they find that

$$F_A = \frac{1}{2(1+\eta)} \left( I_{(5)11}^+ + \sqrt{2\eta} I_{(5)10}^+ \right). \quad (152)$$

Frederico, Henley, and Miller (FHM) use the behavior of the matrix elements in the non-relativistic limit to determine that the bad element is  $I_{(5)10}^+$  [11]. This means that

$$F_A = \frac{1}{2} I_{(5)11}^+. \quad (153)$$

The current matrix elements are calculated using the nucleon axial current. The general form of nucleon axial current is given by [11],

$$J_{(5)n}^\mu = \gamma^\mu \gamma^5 F_A^n + q^\mu \gamma^5 F_P^n. \quad (154)$$

Since we choose to  $\mu = +$  and work in the Breit frame, where  $q^+ = 0$ , Eq. (154) reduces to

$$J_{(5)n}^+ = \gamma^+ \gamma^5 F_A^n. \quad (155)$$

The light-front spinor matrix elements of Eq. (155) can be computed using expressions given in the Appendix. The result is

$$\langle k', \lambda' | J_{(5)n}^+(\mathbf{q}_\perp) | k, \lambda \rangle = \frac{k^+}{M} F_A^n(q) \chi_{\lambda'} \sigma^3 \chi_\lambda. \quad (156)$$

We consider only one model for the nucleon axial form factor since the deuteron axial current has such a simple dependence on it. We choose to use the dipole model

$$F_A(Q^2) = \frac{F_A(0)}{\left(1 + \frac{Q^2}{M_A^2}\right)^2}, \quad (157)$$

where  $M_A$  is the axial mass. For our calculations, we use the value for the axial mass determined by Liesenfeld *et al.* [71].

## V. RESULTS FOR THE FORM FACTORS

We use the deuteron wave functions obtained for the light-front nucleon-nucleon potential in section II to calculate the deuteron currents and form factors. This gives a solution where light-front dynamics is used consistently throughout. For the potential, we choose the light-front nucleon-nucleon potential with  $f_\sigma = 1.2815$ . We have verified that the results do not change significantly when  $f_\sigma = 1.22$  is used.

Figure 11 show the currents and the associated angular condition for  $I_{(1)}^+$ , given by Eq. (144), for several different deuteron wave functions. Results are shown for the wave function from the OME, OME+TME, and OME+TPE potentials (calculated in section II), and the parameterization of the deuteron wave function for the energy independent Bonn potential [22]. The currents matrix elements (but not  $\Delta$ ) are approximately the same regardless of which wave function is used. This consistency is important, since it verifies that the gross features of all the models are the same.

We find that  $\Delta$  for  $I_{(1)}^+$  is much smaller than the largest matrix elements when using the OME wave function. This means that the  $I_{(1)}^+$  current transforms very well under rotations. This is somewhat surprising, since we found earlier that the binding energies for the OME wave functions have a large splitting, indicating that OME wave functions transforms poorly under rotations.

Comparing the current calculated with the OME wave function to those calculated with other potentials, we find that for momentum transfers of more than 1 GeV<sup>2</sup> the OME  $I_{(1)}^+$  current has the best transformation properties under rotation of all the  $I_{(1)}^+$  currents shown.

For smaller momentum transfers, the transformation properties of the Bonn and OME+TME wave functions are the best. This is expected, since in the limit of no momentum transfer, the current  $I_{(1)m'm}^+$  is simply the overlap of deuteron wave functions,  $\langle m' | m \rangle$ . If the initial and final states have the same mass, the matrix element is simply  $\delta_{m'm}$ , which satisfies the angular condition. However, if the states do not have the same mass (which implies that  $m' \neq m$ ), there will be a non-zero overlap between the two states, which violates



the angular condition. Since the masses of the deuteron states are exactly the same for the Bonn wave function, and approximately the same for the OME+TPE wave function, they have a small  $\Delta$  at low momentum transfer. However, the OME wave functions, having the largest mass splitting, have the largest  $\Delta$  at low momentum transfers.

Figures 12 and 13 show the current matrix elements and the angular condition for  $I_{(2)}^+$  and  $I_{(5)}^+$ , respectively. The general features of these figures are the same as in Figure 11, with one important exception. In both figures, the  $\Delta$  for the OME wave function has about the same magnitude as the  $\Delta$ 's for the other wave functions. This means that the rotational properties of  $I_{(2)}^+$  and  $I_{(5)}^+$  currents are approximately the same regardless of which wave function is used. This is a surprising result since it indicates that the rotational properties of the current depend more on how the current is constructed than on which wave function is used.

In Fig. 12, we find that the magnitude of  $\Delta$  is almost the same as the magnitude of the largest matrix element of  $I_{(1)}^+$ . This means there is a large deviation from the angular condition, and that form factors calculated with this current may depend strongly on which matrix element is chosen as “bad”. We show below that this is not the case for the electromagnetic form factors.

We find that  $\Delta$  is much smaller than the largest matrix element of the axial currents shown in Fig. 13 for most values of momentum transfer. This means that the deuteron axial form factor will be essentially independent of which matrix element is chosen as “bad”, except for within the range of 1.5 to 2 GeV<sup>2</sup>.

Now we combine the two parts of the electromagnetic current,  $I_{(1)}^+$  and  $I_{(2)}^+$ , with the nucleon form factors  $F_1$  and  $F_2$  to get the total current. Figure 14 shows the currents for  $F_1 I_{(1)}^+$  and  $F_2 I_{(2)}^+$ , as well as the sum,  $I^+$ . The Gari:1985 nucleon form factors are used [65]. We find that  $F_1 I_{(1)}^+$  gives the largest contribution to the total current, and because  $\Delta$  is small for  $I_{(1)}^+$ ,  $\Delta$  is also small for the total current, meaning that the total current transforms well under rotations. Thus, in spite of the fact that  $\Delta$  is approximately the same size as the current matrix elements for  $I_{(2)}^+$ , the deuteron electromagnetic form factors should not depend too strongly on the choice of the “bad” matrix element. This is especially true for the form factors calculated with the OME wave function.

We calculate the form factors  $A$ ,  $B$ ,  $T_{20}$ , and  $F_A$  using the OME wave function, and show the results in Fig. 15. In general, the form factors do not depend strongly on which matrix element is chosen as “bad”, in agreement with what we predicted in the previous paragraph. The definitions of the “bad” matrix elements are given in sections IV A 4 and IV B. The only exception is for the  $B$  form factor, and to a lesser extent the  $F_A$  form factor, near where they cross zero. This is not too surprising, since a small constant shift in any function near a zero-crossing has a large effect in a logarithmic plot. Also, we note that the FFS and CCKP choices of the “bad” matrix element give the same value for  $B$ . This is a consequence of Eqs. (122) and (123).

We also use the OME+TME wave function to calculate the form factors  $A$ ,  $B$ ,  $T_{20}$ , and  $F_A$ , which we show in Fig. 16. We argued earlier that these electromagnetic form factors depend more strongly on which matrix element is chosen as “bad” than those calculated with the OME wave function, and that dependence is clear in this figure. At low momentum transfers, the dependence on the change is fairly small, but as the momentum transfer increases, so does the dependence. The axial form factor is not affected as strongly, primarily because each wave function generates an axial current which violates the angular condition by approximately the same amount.

Since there are many different models of the nucleon electromagnetic form factors, we calculate the deuteron electromagnetic form factors using each of them to see what effect the differences have. The results are shown in Fig. 17. At low momentum transfers, all the nucleon form factors give close to the same results. However, when the momentum transfers is large, we find a large spread in the values due to nucleon form factors. In fact, this spread is larger than the spread of values obtained from using different “bad” matrix elements with the OME+TME wave functions. In other words, in order to obtain accurate results for momentum transfers over  $2 \text{ GeV}^2$ , it is more important to determine which nucleon form factor to use than when “bad” matrix to use.

Finally, in Fig. 18, we compare the  $A$ ,  $B$ ,  $T_{20}$ , and  $F_A$  form factors for the OME and OME+TME wave functions to experimental data. The “bad” component was chosen according to FFS, and the nucleon form factors of Lomon were used for  $A$ ,  $B$ , and  $T_{20}$ , while the Liesenfeld axial nucleon form factor was used for  $F_A$ . The data for  $A$  is from: Buchanan *et al.* [72], Elias *et al.* [73], Galster *et al.* [74], Platchkov *et al.* [75], Abbott *et al.* [76], and Alexa *et al.* [1]; the data for  $B$  is from: Buchanan *et al.* [72], Auffret *et al.* [77], and Bosted *et al.* [78]; and the data for  $T_{20}$  is from: Schulze *et al.* [79], Gilman *et al.* [80], Boden *et al.* [81], Garcon *et al.* [82], Ferro-Luzzi *et al.* [83], Bouwhuis *et al.* [84], and Abbott *et al.* [85].

There is a rather large difference between the form factors calculated with the OME and OME+TME wave functions. This difference is due primarily to the fact that the OME wave functions are more deeply bound than the OME+TME wave functions, and it can be reduced by choosing a different sigma coupling constant  $f_\sigma$  for the OME and OME+TME potentials. However, for our analysis of rotational invariance, it is important to keep  $f_\sigma$  fixed.

The difference between the calculated form factors and the data is also quite large. This is not unexpected, since in our model of the current, meson exchange currents are not included. It is known that these have a large effect on the form factors at large momentum transfers [57, 86, 87]. Including these effects would bring the form factors into better agreement with the data. However, we emphasize again that agreement with the data is not a priority of this work. Our goal is to gain a better understanding of the breaking of rotational invariance by the light front, and how to restore that invariance. Only after we have that understanding can we pursue accurate calculation of the form factors with light-front dynamics.

## VI. CONCLUSIONS

The issue of rotational invariance in light-front dynamics must be addressed before one attempt to use light-front dynamics for high-precision calculations. In this paper, we have sought to find ways to quantify the level to which rotational invariance is broken. In addition, we have investigated potentials of different orders, since we know that if all orders of the potential were included, rotational invariance would be restored. We have used light-front dynamics to obtain new light-front nucleon-nucleon one-meson-exchange (OME) and two-meson-exchange (TME) potentials.

In section II, we derive OME and TME potentials for a model Lagrangian for nuclear physics which includes chiral symmetry. These potentials are then used in section III to calculate the binding energy and wave function for the  $m = 0$  and  $m = 1$  states of the deuteron. We find that the splitting between the  $m = 0$  and  $m = 1$  states was smaller for the OME+TME potential as compared to the OME potential gives.

In section V, the wave functions obtained in section II are used to calculate the form

factors of the deuteron using only light-front dynamics throughout. In light-front dynamics, there are four independent components of the deuteron current. However, the requirement of rotational invariance introduces an angular condition that the four components must satisfy, reducing the number of physically independent components to three. The deviation of the calculated current components from the angular condition is denoted by  $\Delta$ . We find that  $\Delta$  is very small for the deuteron wave functions calculated with the OME potential. This is an important result, since it means that although *in principle* the light-front calculation of the deuteron current does not transform correctly under rotations, *in practice* it does quite well. The smallness of  $\Delta$  means that any reasonable prescription for eliminating the dependent component of the current gives essentially the same results; the uncertainty introduced by the various nucleon form factors is much greater.

We also found that  $\Delta$  is significantly larger when the TME potentials are used. Since the results in Refs. [18, 19, 48] indicate that the rotational properties of the TME wave function are better than for the OME wave function, we interpret the increase in  $\Delta$  as an indication that extra diagrams need to be included in the current calculation to restore rotational invariance. That is, having a wave function with good rotational properties is not sufficient to obtain matrix elements of the current operator with good rotational properties. To verify this, the contribution to the deuteron form factors due to the photon coupling to an intermediate two-meson-exchange type of diagram must be calculated. This may restore the rotational invariance of the deuteron form factor when the wave function is calculated using the two-meson-exchange potentials.

## Acknowledgments

This work is supported in part by the U.S. Dept. of Energy under Grant No. DE-FG03-97ER4014. We are grateful to Daniel Phillips for many many useful discussions about this work.

\*

## APPENDIX A: NOTATION, CONVENTIONS, AND USEFUL RELATIONS

For a general four-vector  $a$  with components  $(a^0, a^1, a^2, a^3)$  in the equal-time basis, we define the light-front variables

$$a^\pm = a^0 \pm a^3, \tag{A1}$$

$$\mathbf{a}_\perp = (a^1, a^2), \tag{A2}$$

so the 4-vector  $a^\mu$  can be denoted in the light-front basis as

$$a = (a^+, a^-, \mathbf{a}_\perp). \tag{A3}$$

Using this, we find that the scalar product is

$$a \cdot b = a^\mu b_\mu = \frac{1}{2} (a^+ b^- + a^- b^+) - \mathbf{a}_\perp \cdot \mathbf{b}_\perp. \tag{A4}$$

This defines  $g_{\mu\nu}$ , with  $g_{+-} = g_{-+} = 1/2$ ,  $g_{11} = g_{22} = -1$ , and all other elements of  $g$  vanish. The elements of  $g^{\mu\nu}$  are obtained from the condition that  $g^{\mu\nu}$  is the inverse of  $g_{\mu\nu}$ , so

$g^{\alpha\beta}g_{\beta\lambda} = \delta_{\lambda}^{\alpha}$ . Its elements are the same as those of  $g_{\mu\nu}$ , except that  $g^{-+} = g^{+-} = 2$ . Thus,

$$a^{\pm} = 2a_{\mp}. \quad (\text{A5})$$

and the partial derivatives are similarly given by

$$\partial^{\pm} = 2\partial_{\mp} = 2\frac{\partial}{\partial x^{\mp}}. \quad (\text{A6})$$

To find the physical consequences of this coordinate system, consider the commutation relations  $[p^{\mu}, x^{\nu}] = ig^{\mu\nu}$ , which yield

$$[p^{\pm}, x^{\mp}] = 2i, \quad (\text{A7})$$

$$[\mathbf{p}_{\perp}^i, \mathbf{x}_{\perp}^j] = -i\delta_{i,j}, \quad (\text{A8})$$

with the other commutators equal to zero. This means that  $\mathbf{x}_{\perp}^i$  is canonically conjugate to  $\mathbf{p}_{\perp}^i$ , and  $x^{\pm}$  is conjugate to  $p^{\mp}$ . Since  $x^+$  plays the role of time (the light-front time) in light-front dynamics, and  $p^-$  is canonically conjugate to  $x^+$ , this means that  $p^-$  is the light-front energy and that the light-front Hamiltonian is given by  $P^-$ .

In any Hamiltonian theory, particles have the an energy defined by the on-shell constraint  $k^2 = m^2$ . This implies that the light-front energy of a particle is

$$k^- = \frac{m^2 + \mathbf{k}_{\perp}^2}{k^+}. \quad (\text{A9})$$

The independent components of the momentum can be written as a light-front three-vector  $\mathbf{k}_{\text{LF}}$ , denoted by

$$\mathbf{k}_{\text{LF}} = (k^+, \mathbf{k}_{\perp}). \quad (\text{A10})$$

For dealing with spin, we require the Pauli sigma matrices, which are

$$(\sigma^1, \sigma^2, \sigma^3) = \left( \left( \begin{array}{cc} 0 & 1 \\ 1 & 0 \end{array} \right), \left( \begin{array}{cc} 0 & -i \\ i & 0 \end{array} \right), \left( \begin{array}{cc} 1 & 0 \\ 0 & -1 \end{array} \right) \right). \quad (\text{A11})$$

The Bjorken and Drell convention [63] for the gamma matrices is used in this work. They specify that

$$\gamma^0 = \beta = \left( \begin{array}{cc} 1 & 0 \\ 0 & -1 \end{array} \right), \quad (\text{A12})$$

$$\boldsymbol{\gamma} = \beta\boldsymbol{\alpha} = \left( \begin{array}{cc} 0 & \boldsymbol{\sigma} \\ -\boldsymbol{\sigma} & 0 \end{array} \right), \quad (\text{A13})$$

$$\gamma^5 = i\gamma^0\gamma^1\gamma^2\gamma^3 = \left( \begin{array}{cc} 0 & 1 \\ 1 & 0 \end{array} \right). \quad (\text{A14})$$

The spin matrices  $S^i$  then are

$$S^i = \frac{1}{2}\Sigma^i = -\frac{1}{2}\gamma^5\gamma^i, \quad (\text{A15})$$

$$\Sigma^i = \left( \begin{array}{cc} \sigma^i & 0 \\ 0 & -\sigma^i \end{array} \right). \quad (\text{A16})$$

Using  $\Sigma$ , we can express the helicity operator as  $H = \hat{p} \cdot \Sigma$ , which has eigenvalues  $\pm 1$ . This is useful since the helicity is invariant under rotations.

It is useful to define the spinor projection operators  $\Lambda_{\pm}$  by

$$\Lambda_{\pm} = \frac{1}{4} \gamma^{\mp} \gamma^{\pm} = \frac{1}{2} \gamma^0 \gamma^{\pm} = \frac{1}{2} (I \pm \alpha^3). \quad (\text{A17})$$

These satisfy the requirements for projection operators,

$$\Lambda_+ + \Lambda_- = 1, \quad (\text{A18})$$

$$(\Lambda_{\pm})^2 = \Lambda_{\pm}, \quad (\text{A19})$$

$$\Lambda_{\pm} \Lambda_{\mp} = 0. \quad (\text{A20})$$

We summarize the effect these projection operators have on the gamma matrices:

$$\Lambda_{\pm} \gamma^0 = \gamma^0 \Lambda_{\mp}, \quad (\text{A21})$$

$$\Lambda_{\pm} \gamma^{\pm} = 0 = \gamma^{\pm} \Lambda_{\mp}, \quad (\text{A22})$$

$$\Lambda_{\pm} \gamma^{\mp} = \gamma^{\mp} = \gamma^{\mp} \Lambda_{\mp}, \quad (\text{A23})$$

$$\Lambda_{\pm} \gamma^{\perp} = \gamma^{\perp} \Lambda_{\pm}, \quad (\text{A24})$$

and under conjugation,

$$\gamma^0 \Lambda_{\pm}^{\dagger} \gamma^0 = \Lambda_{\mp}. \quad (\text{A25})$$

The spinors used by Bjorken and Drell [63] are polarized in the  $\hat{z}$  direction, and so the  $\chi$ 's are chosen to be

$$\chi_{+1/2} = \begin{pmatrix} 1 \\ 0 \end{pmatrix}, \quad (\text{A26})$$

$$\chi_{-1/2} = \begin{pmatrix} 0 \\ 1 \end{pmatrix}. \quad (\text{A27})$$

The light-front spinors are defined to be [6]

$$u_{\text{LF}}(k, \lambda) \equiv \frac{1}{\sqrt{Mk^+}} \left[ M \Lambda_- + (k^+ + \boldsymbol{\alpha}^{\perp} \cdot \mathbf{k}^{\perp}) \Lambda_+ \right] \chi_{\text{LF}, \lambda} \quad (\text{A28})$$

$$= \frac{1}{\sqrt{Mk^+}} \left[ \Lambda_- (M + \boldsymbol{\alpha}^{\perp} \cdot \mathbf{k}^{\perp}) + \Lambda_+ k^+ \right] \chi_{\text{LF}, \lambda}, \quad (\text{A29})$$

$$\chi_{\text{LF}, \lambda} \equiv \begin{pmatrix} \chi_{\lambda} \\ 0 \end{pmatrix}, \quad (\text{A30})$$

where  $\chi_{\lambda}$  is the usual Pauli spinor, and the  $\Lambda_{\pm}$  are the spinor projection operators defined in Eq. (A17). We find that

$$\bar{u}_{\text{LF}}(k, \lambda) = \frac{1}{\sqrt{Mk^+}} \chi_{\text{LF}, \lambda}^{\dagger} \left[ \Lambda_+ M + \Lambda_- (k^+ + \boldsymbol{\alpha}^{\perp} \cdot \mathbf{k}^{\perp}) \right] \quad (\text{A31})$$

$$= \frac{1}{\sqrt{Mk^+}} \chi_{\text{LF}, \lambda}^{\dagger} \left[ (M - \boldsymbol{\alpha}^{\perp} \cdot \mathbf{k}^{\perp}) \Lambda_+ + k^+ \Lambda_- \right]. \quad (\text{A32})$$

Note that these spinors are normalized to satisfy  $\bar{u}_{\text{LF}}(k, \lambda') u_{\text{LF}}(k, \lambda) = \delta_{\lambda'\lambda}$ .

For helicity spinors, we choose the eigenvectors of the helicity operator  $(\boldsymbol{\sigma} \cdot \hat{\boldsymbol{p}})$  as the  $\chi$ 's. In particular,  $(\hat{\boldsymbol{p}} \cdot \boldsymbol{\Sigma})u(\boldsymbol{p}, \lambda) = hu(\boldsymbol{p}, \lambda)$ , where  $h = 2\lambda$ . This choice allows us to write

$$u(\boldsymbol{p}, \lambda) = \sqrt{\frac{W}{2M}} \begin{pmatrix} 1 \\ f \end{pmatrix} \chi_{\lambda}(\hat{\boldsymbol{p}}), \quad (\text{A33})$$

and

$$\chi_{\lambda}(\hat{\boldsymbol{p}}) = \begin{cases} \begin{pmatrix} c_2 e^{-i\phi/2} \\ s_2 e^{+i\phi/2} \end{pmatrix} & \text{if } h = +1 \\ \begin{pmatrix} -s_2 e^{-i\phi/2} \\ c_2 e^{+i\phi/2} \end{pmatrix} & \text{if } h = -1 \end{cases} \quad (\text{A34})$$

where  $c_2 = \cos \frac{\theta}{2}$ ,  $s_2 = \sin \frac{\theta}{2}$ ,  $f = \frac{hp}{W}$ , and  $h = 2\lambda$ .

When there are two fermions in the center-of-momentum frame, we can define  $\phi \equiv \phi_1$  and  $\theta \equiv \theta_1$  and for particle two  $\phi_2 = \pi + \phi$  and  $\theta_2 = \pi - \theta$ . This means that

$$u(\boldsymbol{p}_i, \lambda_i) = \sqrt{\frac{W}{2M}} \begin{pmatrix} 1 \\ f_i \end{pmatrix} \chi_{i, \lambda_i}(\hat{\boldsymbol{p}}), \quad (\text{A35})$$

where  $i = 1, 2$  and

$$\chi_{1, \lambda_1}(\hat{\boldsymbol{p}}) = \chi_{\lambda_1}(\hat{\boldsymbol{p}}), \quad (\text{A36})$$

$$\chi_{2, \lambda_2}(\hat{\boldsymbol{p}}) = i\chi_{-\lambda_2}(\hat{\boldsymbol{p}}). \quad (\text{A37})$$

- 
- [1] Jefferson Lab Hall A, L. C. Alexa *et al.*, Phys. Rev. Lett. **82**, 1374 (1999), nucl-ex/9812002.
  - [2] P. A. M. Dirac, Rev. Mod. Phys. **21**, 392 (1949).
  - [3] S. J. Brodsky, H.-C. Pauli, and S. S. Pinsky, Phys. Rept. **301**, 299 (1998), hep-ph/9705477.
  - [4] A. Harindranath, (1996), hep-ph/9612244.
  - [5] T. Heinzl, (1998), hep-th/9812190.
  - [6] G. A. Miller, Phys. Rev. **C56**, 2789 (1997), nucl-th/9706028.
  - [7] G. A. Miller, Prog. Part. Nucl. Phys. **45**, 83 (2000), nucl-th/0002059.
  - [8] This problem is not unique to light-front dynamics. In any form of Hamiltonian dynamics, at least three of the Poincaré group generators are dynamic, and thus complicated.
  - [9] U. Trittman and H.-C. Pauli, (1997), hep-th/9705021.
  - [10] L. L. Frankfurt, T. Frederico, and M. Strikman, Phys. Rev. **C48**, 2182 (1993).
  - [11] T. Frederico, E. M. Henley, and G. A. Miller, Nucl. Phys. **A533**, 617 (1991).
  - [12] L. A. Kondratyuk and M. I. Strikman, Nucl. Phys. **A426**, 575 (1984).
  - [13] F. Cardarelli, I. L. Grach, I. M. Narodetsky, G. Salme, and S. Simula, Phys. Lett. **B349**, 393 (1995), hep-ph/9502360.
  - [14] D. Arndt and C.-R. Ji, Phys. Rev. **D60**, 094020 (1999), hep-ph/9905360.
  - [15] J. Carbonell and V. A. Karmanov, In *Williamsburg 1994, Few-body problems in physics* 891-894.

- [16] J. Carbonell and V. A. Karmanov, Nucl. Phys. **A581**, 625 (1995).
- [17] P. L. Chung, W. N. Polyzou, F. Coester, and B. D. Keister, Phys. Rev. **C37**, 2000 (1988).
- [18] J. R. Cooke, G. A. Miller, and D. R. Phillips, Phys. Rev. **C61**, 064005 (2000), nucl-th/9910013.
- [19] J. R. Cooke and G. A. Miller, Phys. Rev. **C62**, 054008 (2000), nucl-th/0002016.
- [20] G. A. Miller and R. Machleidt, Phys. Rev. **C60**, 035202 (1999), nucl-th/9903080.
- [21] F. Gursey, Nuovo Cim. **16**, 230 (1960).
- [22] R. Machleidt, K. Holinde, and C. Elster, Phys. Rept. **149**, 1 (1987).
- [23] R. Machleidt, One-boson-exchange potentials and nucleon-nucleon scattering, in *Computational Nuclear Physics 2—Nuclear Reactions*, edited by K. Langanke, J. A. Maruhn, and S. E. Koonin, chap. 1, p. 1, Springer, New York, 1993.
- [24] D. Black, A. H. Fariborz, F. Sannino, and J. Schechter, Phys. Rev. **D59**, 074026 (1999), hep-ph/9808415.
- [25] D. Black, A. H. Fariborz, and J. Schechter, Phys. Rev. **D61**, 074030 (2000), hep-ph/9910351.
- [26] D. Black, A. H. Fariborz, S. Moussa, S. Nasri, and J. Schechter, Phys. Rev. **D64**, 014031 (2001), hep-ph/0012278.
- [27] G. A. Miller, Phys. Rev. **C56**, 8 (1997), nucl-th/9702036.
- [28] S.-J. Chang, R. G. Root, and T.-M. Yan, Phys. Rev. **D7**, 1133 (1973).
- [29] S.-J. Chang and T.-M. Yan, Phys. Rev. **D7**, 1147 (1973).
- [30] T.-M. Yan, Phys. Rev. **D7**, 1760 (1973).
- [31] T.-M. Yan, Phys. Rev. **D7**, 1780 (1973).
- [32] D. E. Soper, SLAC-R-0137.
- [33] J. B. Kogut and D. E. Soper, Phys. Rev. **D1**, 2901 (1970).
- [34] J. D. Bjorken, J. B. Kogut, and D. E. Soper, Phys. Rev. **D3**, 1382 (1971).
- [35] D. E. Soper, Phys. Rev. **D4**, 1620 (1971).
- [36] Y. Nambu, Prog. Theor. Phys. **5**, 614 (1950).
- [37] J. Schwinger, Proc. Nat. Acad. Sci. **37**, 452 (1951).
- [38] J. Schwinger, Proc. Nat. Acad. Sci. **37**, 455 (1951).
- [39] M. Gell-Mann and F. Low, Phys. Rev. **84**, 350 (1951).
- [40] E. E. Salpeter and H. A. Bethe, Phys. Rev. **84**, 1232 (1951).
- [41] N. C. J. Schoonderwoerd and B. L. G. Bakker, Phys. Rev. **D57**, 4965 (1998).
- [42] N. C. J. Schoonderwoerd and B. L. G. Bakker, Phys. Rev. **D58**, 025013 (1998), hep-ph/9801433.
- [43] N. Schoonderwoerd, (1998), hep-ph/9811317.
- [44] B. H. Brandsden and R. G. Moorhouse, *The Pion-Nucleon System* (Princeton University Press, Princeton, 1973).
- [45] S. L. Adler and R. F. Dashen, *Current Algebras* (W. A. Benjamin, New York, 1968).
- [46] J. R. Cooke, Ph.D. thesis, University of Washington, 2001, nucl-th/0112029.
- [47] J. Carbonell, B. Desplanques, V. A. Karmanov, and J. F. Mathiot, Phys. Rept. **300**, 215 (1998), nucl-th/9804029.
- [48] J. R. Cooke and G. A. Miller, in preparation.
- [49] E. Hummel and J. A. Tjon, Phys. Rev. **C42**, 423 (1990).
- [50] M. J. Zuilhof and J. A. Tjon, Phys. Rev. **C22**, 2369 (1980).
- [51] G. Rupp and J. A. Tjon, Phys. Rev. **C41**, 472 (1990).
- [52] M. Garcon and J. W. Van Orden, (2001), arXiv:nucl-th/0102049.
- [53] R. G. Arnold, C. E. Carlson, and F. Gross, Phys. Rev. **C23**, 363 (1981).
- [54] F. Coester and A. Ostebee, Phys. Rev. **C11**, 1836 (1975).

- [55] T. E. O. Ericson and M. Rosa-Clot, Nucl. Phys. **A405**, 497 (1983).
- [56] P. J. Mohr and B. N. Taylor, Rev. Mod. Phys. **72**, 351 (2000).
- [57] D. R. Phillips, S. J. Wallace, and N. K. Devine, Phys. Rev. **C58**, 2261 (1998), nucl-th/9802067.
- [58] JLAB t20, D. Abbott *et al.*, Eur. Phys. J. **A7**, 421 (2000), nucl-ex/0002003.
- [59] R. Dashen and M. Gell-Mann, Phys. Rev. Lett. **17**, 340 (1966).
- [60] I. L. Grach and L. A. Kondratyuk, Sov. J. Nucl. Phys. **39**, 198 (1984).
- [61] S. J. Brodsky and J. R. Hiller, Phys. Rev. **D46**, 2141 (1992).
- [62] H. J. Melosh, Phys. Rev. **D9**, 1095 (1974).
- [63] J. D. Bjorken and S. D. Drell, *Relativistic Quantum Mechanics* (McGraw-Hill, Inc., New York, 1964), chap. 3.
- [64] G. Hohler *et al.*, Nucl. Phys. **B114**, 505 (1976).
- [65] M. F. Gari and W. Krümpelmann, Z. Phys. **A322**, 689 (1985).
- [66] M. F. Gari and W. Krümpelmann, Phys. Lett. **B274**, 159 (1992).
- [67] M. F. Gari and W. Krümpelmann, Phys. Lett. **B282**, 483 (1992).
- [68] P. Mergell, U. G. Meissner, and D. Drechsel, Nucl. Phys. **A596**, 367 (1996), hep-ph/9506375.
- [69] E. L. Lomon, Phys. Rev. **C64**, 035204 (2001), nucl-th/0104039.
- [70] K. de Jager, (1999), hep-ex/0003034.
- [71] A1, A. Liesenfeld *et al.*, Phys. Lett. **B468**, 20 (1999), nucl-ex/9911003.
- [72] C. D. Buchanan *et al.*, Phys. Rev. Lett. **15**, 303 (1965).
- [73] J. E. Elias *et al.*, Phys. Rev. **177**, 2075 (1969).
- [74] S. Galster *et al.*, Nucl. Phys. **B32**, 221 (1971).
- [75] S. Platchkov *et al.*, Nucl. Phys. **A510**, 740 (1990).
- [76] Jefferson Lab t(20), D. Abbott *et al.*, Phys. Rev. Lett. **82**, 1379 (1999), nucl-ex/9810017.
- [77] S. Auffret *et al.*, Phys. Rev. Lett. **54**, 649 (1985).
- [78] P. Bosted *et al.*, Phys. Rev. **C42**, 38 (1990).
- [79] M. E. Schulze *et al.*, Phys. Rev. Lett. **52**, 597 (1984).
- [80] R. Gilman *et al.*, Phys. Rev. Lett. **65**, 1733 (1990).
- [81] B. Boden *et al.*, Z. Phys. **C49**, 175 (1991).
- [82] M. Garcon *et al.*, Phys. Rev. **C49**, 2516 (1994).
- [83] M. Ferro-Luzzi *et al.*, Phys. Rev. Lett. **77**, 2630 (1996).
- [84] M. Bouwhuis *et al.*, Phys. Rev. Lett. **82**, 3755 (1999), nucl-ex/9810004.
- [85] JLAB t(20), D. Abbott *et al.*, Phys. Rev. Lett. **84**, 5053 (2000), nucl-ex/0001006.
- [86] R. B. Wiringa, V. G. J. Stoks, and R. Schiavilla, Phys. Rev. **C51**, 38 (1995), nucl-th/9408016.
- [87] R. Schiavilla and D. O. Riska, Phys. Rev. **C43**, 437 (1991).



TABLE I: The parameters for the  $\pi$ ,  $\eta$ ,  $\rho$ ,  $\omega$ ,  $\delta$ , and  $\sigma$  mesons. For the meson type, “iv” and “is” stand for isovector and isoscalar, while “ps”, “v”, and “s” stand for pseudoscalar, vector, and scalar. The  $\sigma$  meson is also known as  $f_0(400 - 1200)$ , and the  $\delta$  meson is the  $a_0(980)$ .

Meson	type	mass [MeV]	$\Lambda$ [GeV]	$n$	$\frac{g^2}{4\pi}$	$\frac{f}{g}$
$\pi$	iv,ps	138.04	1.2	1	14.0	
$\eta$	is,ps	547.5	1.5	1	3.0	
$\rho$	iv,v	769.	1.85	2	0.9	6.1
$\omega$	is,v	782.	1.85	2	24.5	0.0
$\delta$	iv,s	983.	2.0	1	2.0723	
$\sigma$	is,s	550.	2.0	1	$f_\sigma \times 8.9602$	

TABLE II: The values of  $f_\sigma$  required to give the physical value of the deuteron mass for a given potential and state with  $J_z = m$ . The percent of the wave function in the D-state and in the  $J = 1$  state are also shown.

Potential	$f_\sigma$			% D state		% $J = 1$	
	m=0	m=1	Diff	m=0	m=1	m=0	m=1
OME	1.2407	1.2125	0.0282	2.87	3.55	99.99	99.97
OME +TPE	1.2829	1.2819	0.0010	2.96	3.23	99.99	99.97
OME +TME	1.2968	1.3079	-0.0111	2.95	3.28	99.99	99.96
OME +ncTPE	1.3064	1.3121	-0.0057	2.99	3.16	99.98	99.97
OME +ncTME	1.3198	1.3397	-0.0199	2.98	3.21	99.98	99.96

TABLE III: The values of the binding energy, percentage of the wave function in the D state, and the percentage of the wave function in the  $J = 1$  state for the  $m = 0$  and  $m = 1$  states for different potentials. The  $\sigma$  coupling constant factor is  $f_\sigma = 1.22$ .

Potential	Binding Energy (MeV)			D state (%)		$J = 1$ (%)	
	m=0	m=1	Diff	m=0	m=1	m=0	m=1
OME only	-1.7653	-2.4200	0.6547	2.73	3.61	99.99	99.96
OME + $\pi$ -( $\sigma$ - $\omega$ ) Mesa	-1.9236	-1.7021	-0.2215	2.80	3.38	99.99	99.96
OME +ncTME	-0.4948	-0.2646	-0.2302	1.97	1.76	99.99	99.98
OME +ncTPE	-0.6620	-0.4825	-0.1795	2.16	2.09	99.99	99.98
OME +TME	-0.7861	-0.6060	-0.1801	2.25	2.31	99.99	99.97
OME +TPE	-0.9981	-0.9155	-0.0826	2.42	2.57	99.99	99.98

TABLE IV: The values of the binding energy, percentage of the wave function in the D state, and the percentage of the wave function in the  $J = 1$  state for the  $m = 0$  and  $m = 1$  states for different potentials. The  $\sigma$  coupling constant factor is  $f_\sigma = 1.2815$ , distinguishes this table from Table III.

Potential	Binding Energy (MeV)			D state (%)		$J = 1$ (%)	
	m=0	m=1	Diff	m=0	m=1	m=0	m=1
OME only	-3.3500	-4.4546	1.1046	3.09	3.97	99.99	99.96
OME + $\pi$ -( $\sigma$ - $\omega$ ) Mesa	-3.6331	-3.2408	-0.3923	3.10	3.85	99.99	99.95
OME +ncTME	-1.3766	-0.9901	-0.3865	2.67	2.64	99.99	99.97
OME +ncTPE	-1.6532	-1.4693	-0.1839	2.81	2.88	99.99	99.97
OME +TME	-1.8617	-1.6032	-0.2585	2.85	3.05	99.99	99.96
OME +TPE	-2.1915	-2.2137	0.0222	2.95	3.23	99.99	99.97

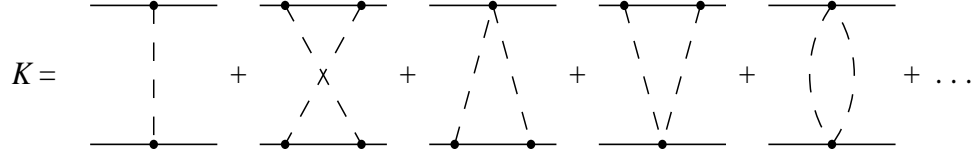


FIG. 1: The first several terms of the full kernel for the Bethe-Salpeter equation of the nuclear model with chiral symmetry.

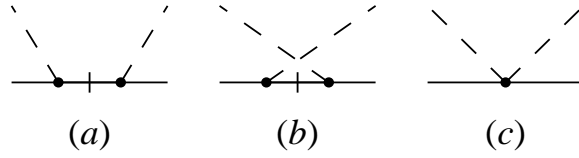


FIG. 2: The non-vanishing diagrams for pion-nucleon scattering at threshold: (a)  $\mathcal{M}_U$ , (b)  $\mathcal{M}_X$ , and (c)  $\mathcal{M}_C$ . The mesons here are pions.

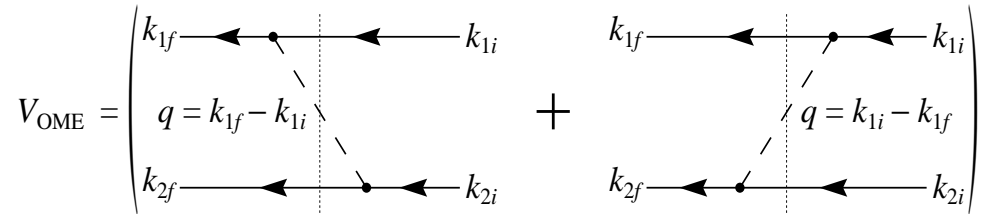


FIG. 3: The two diagrams which contribute to the OME potential for each meson.

$$\begin{aligned}
(a) \quad V_{\text{TME:M}} &= \left( \begin{array}{c} \begin{array}{c} k_{1f} \leftarrow \text{---} \bullet \text{---} k_{1m} \text{---} \bullet \text{---} k_{1i} \\ \text{---} \bullet \text{---} k_{2f} \text{---} \bullet \text{---} k_{2m} \text{---} \bullet \text{---} k_{2i} \end{array} \\ q_f = k_{1m} - k_{1f} \quad q_i = k_{1m} - k_{1i} \end{array} \right) + \left( \begin{array}{c} \begin{array}{c} k_{1f} \leftarrow \text{---} \bullet \text{---} k_{1m} \text{---} \bullet \text{---} k_{1i} \\ \text{---} \bullet \text{---} k_{2f} \text{---} \bullet \text{---} k_{2m} \text{---} \bullet \text{---} k_{2i} \end{array} \\ q_f = k_{2m} - k_{2f} \quad q_i = k_{2m} - k_{2i} \end{array} \right) \\
(b) \quad V_{\text{TME:SB}} &= \left( \begin{array}{c} \begin{array}{c} k_{1f} \leftarrow \text{---} \bullet \text{---} k_{1m} \text{---} \bullet \text{---} k_{1i} \\ \text{---} \bullet \text{---} k_{2f} \text{---} \bullet \text{---} k_{2m} \text{---} \bullet \text{---} k_{2i} \end{array} \\ q_f = k_{1f} - k_{1m} \quad q_i = k_{1m} - k_{1i} \end{array} \right) + \left( \begin{array}{c} \begin{array}{c} k_{1f} \leftarrow \text{---} \bullet \text{---} k_{1m} \text{---} \bullet \text{---} k_{1i} \\ \text{---} \bullet \text{---} k_{2f} \text{---} \bullet \text{---} k_{2m} \text{---} \bullet \text{---} k_{2i} \end{array} \\ q_f = k_{2f} - k_{2m} \quad q_i = k_{2m} - k_{2i} \end{array} \right) \\
(c) \quad V_{\text{TME:SBI}} &= \left( \begin{array}{c} \begin{array}{c} k_{1f} \leftarrow \text{---} \bullet \text{---} k_{1m} \text{---} \bullet \text{---} k_{1i} \\ \text{---} \bullet \text{---} k_{2f} \text{---} \bullet \text{---} k_{2m} \text{---} \bullet \text{---} k_{2i} \end{array} \\ q_f = k_{1f} - k_{1m} \quad q_i = k_{1m} - k_{1i} \end{array} \right) + \left( \begin{array}{c} \begin{array}{c} k_{1f} \leftarrow \text{---} \bullet \text{---} k_{1m} \text{---} \bullet \text{---} k_{1i} \\ \text{---} \bullet \text{---} k_{2f} \text{---} \bullet \text{---} k_{2m} \text{---} \bullet \text{---} k_{2i} \end{array} \\ q_f = k_{2f} - k_{2m} \quad q_i = k_{2m} - k_{2i} \end{array} \right) \\
+ \left( \begin{array}{c} \begin{array}{c} k_{1f} \leftarrow \text{---} \bullet \text{---} k_{1m} \text{---} \bullet \text{---} k_{1i} \\ \text{---} \bullet \text{---} k_{2f} \text{---} \bullet \text{---} k_{2m} \text{---} \bullet \text{---} k_{2i} \end{array} \\ q_f = k_{1f} - k_{1m} \quad q_i = k_{1m} - k_{1i} \end{array} \right) + \left( \begin{array}{c} \begin{array}{c} k_{1f} \leftarrow \text{---} \bullet \text{---} k_{1m} \text{---} \bullet \text{---} k_{1i} \\ \text{---} \bullet \text{---} k_{2f} \text{---} \bullet \text{---} k_{2m} \text{---} \bullet \text{---} k_{2i} \end{array} \\ q_f = k_{2f} - k_{2m} \quad q_i = k_{2m} - k_{2i} \end{array} \right) \\
(d) \quad V_{\text{TME:SBI}} &= \left( \begin{array}{c} \begin{array}{c} k_{1f} \leftarrow \text{---} \bullet \text{---} k_{1m} \text{---} \bullet \text{---} k_{1i} \\ \text{---} \bullet \text{---} k_{2f} \text{---} \bullet \text{---} k_{2m} \text{---} \bullet \text{---} k_{2i} \end{array} \\ q_f = k_{1f} - k_{1m} \quad q_i = k_{1m} - k_{1i} \end{array} \right) + \left( \begin{array}{c} \begin{array}{c} k_{1f} \leftarrow \text{---} \bullet \text{---} k_{1m} \text{---} \bullet \text{---} k_{1i} \\ \text{---} \bullet \text{---} k_{2f} \text{---} \bullet \text{---} k_{2m} \text{---} \bullet \text{---} k_{2i} \end{array} \\ q_f = k_{2f} - k_{2m} \quad q_i = k_{2m} - k_{2i} \end{array} \right)
\end{aligned}$$

FIG. 4: The TME potentials for (a)  $V_{\text{TME:M}}$  (the Mesa potential), (b)  $V_{\text{TME:SB}}$  (the stretched box potential), (c)  $V_{\text{TME:SBI}}$  (the stretched instantaneous potential), and (d)  $V_{\text{TME:SBI}}$  (the stretched double instantaneous potential). Note that the graphs on the right side are obtained from the graphs on the left side by  $1 \leftrightarrow 2$ .



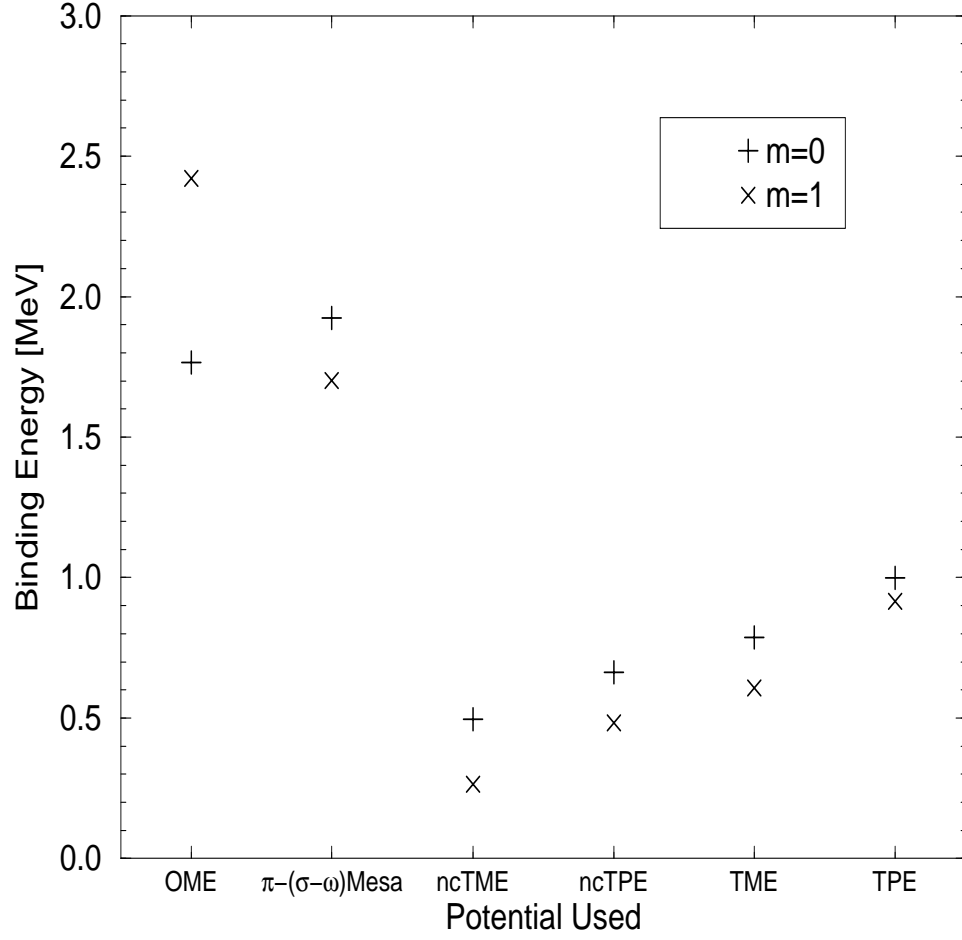


FIG. 6: The values of the binding energy for the  $m = 0$  and  $m = 1$  states for different nucleon-nucleon light-front potentials. The  $\sigma$  coupling constant factor is  $f_\sigma = 1.22$ .

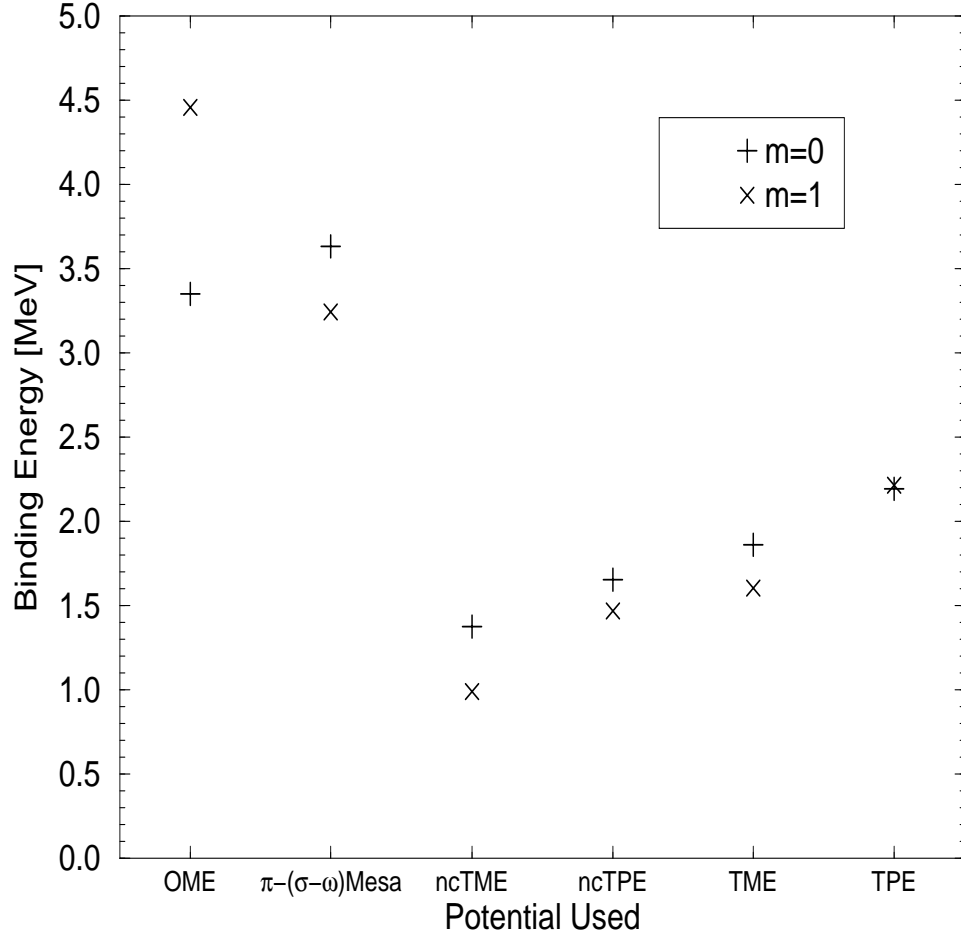


FIG. 7: The values of the binding energy for the  $m = 0$  and  $m = 1$  states for different nucleon-nucleon light-front potentials. The  $\sigma$  coupling constant factor is  $f_\sigma = 1.2815$ .

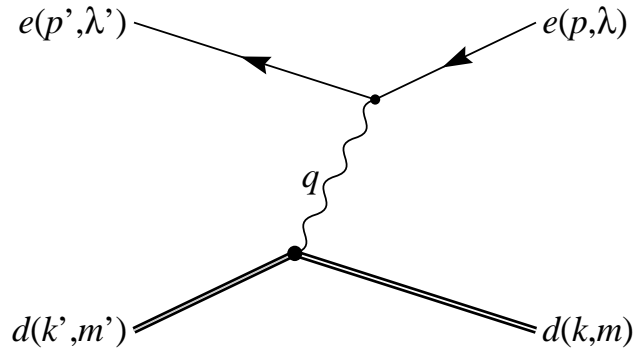


FIG. 8: The Feynman diagram for one-photon-exchange electron-deuteron scattering.

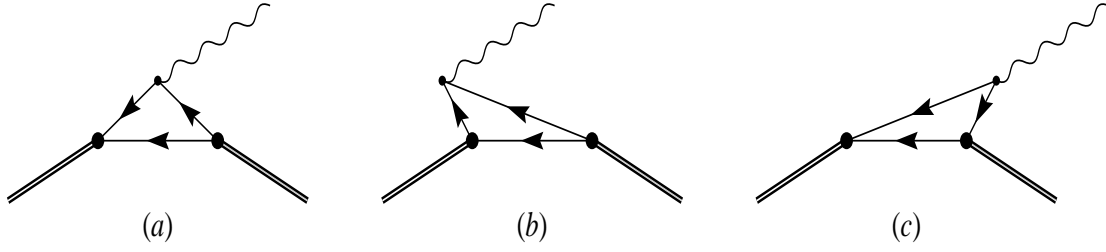


FIG. 9: The lowest-order graphs which contribute to the deuteron current matrix element.

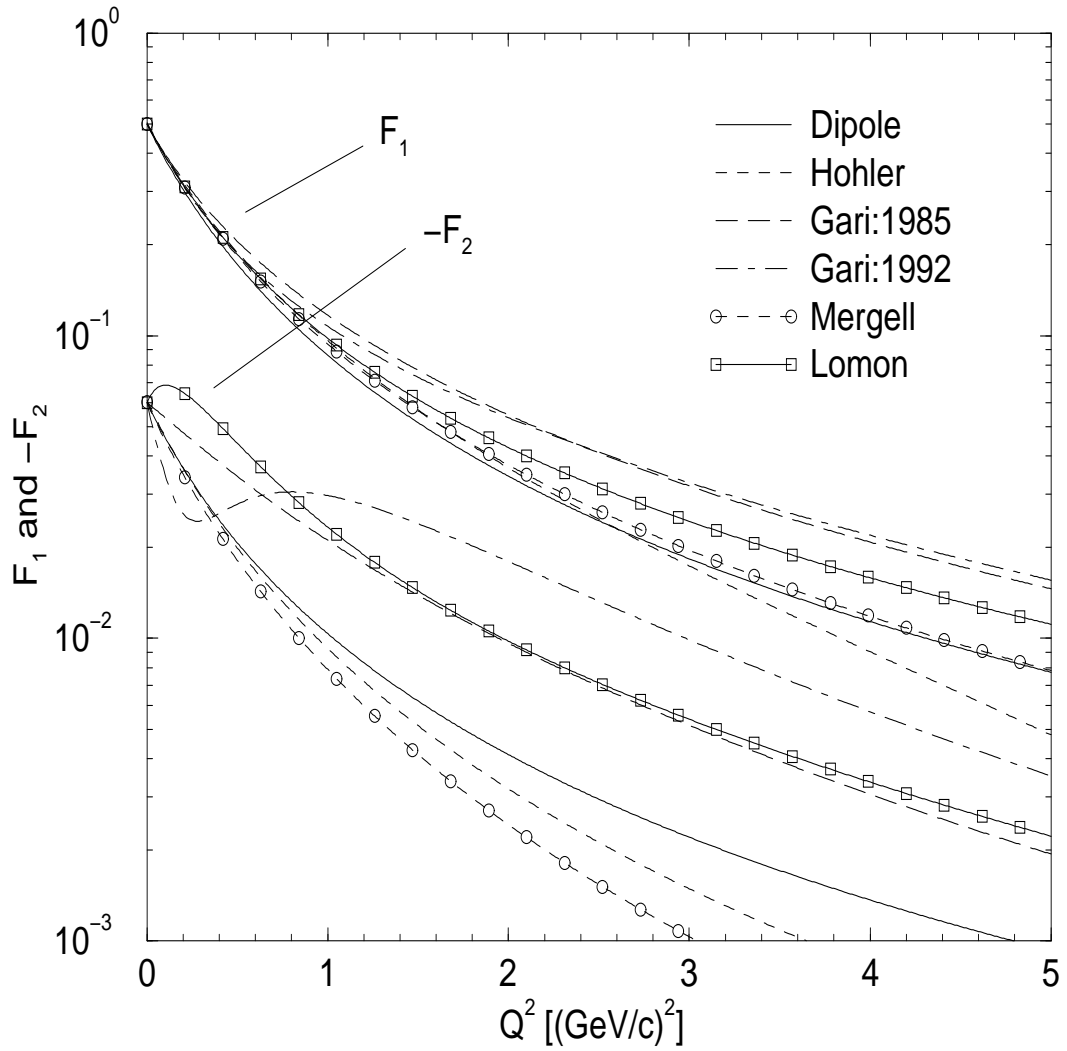


FIG. 10: The  $F_1$  and  $-F_2$  isoscalar nucleon form factors for six different models: the dipole model, Hohler, Gari:1985, Gari:1992, Mergell, and Lomon.



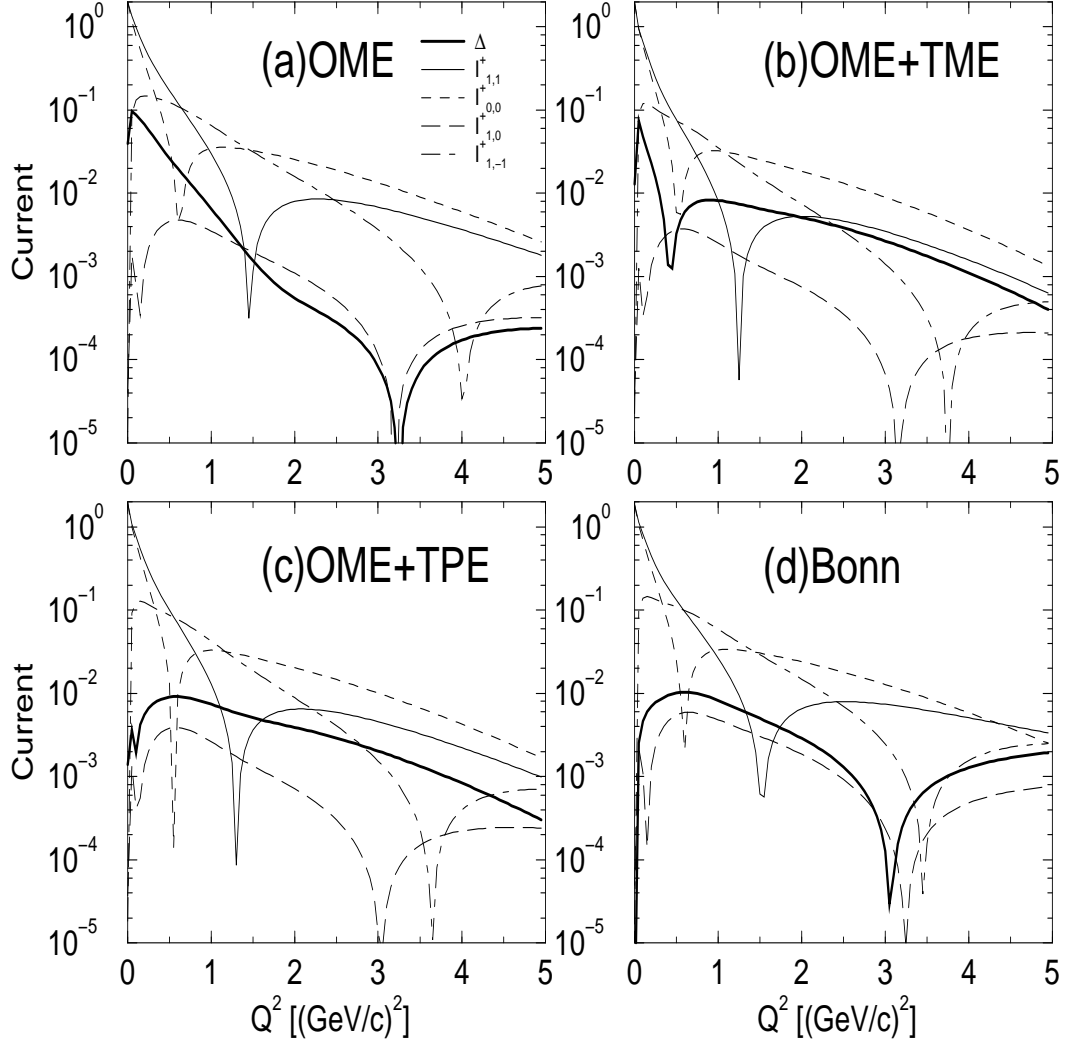


FIG. 11: The matrix elements of  $I_{(1)m'm}^+$ , the component of the electromagnetic current which multiplies the nucleon  $F_1$  form factor, calculated with the wave function from the (a) OME, (b) OME+TME, (c) OME+TPE, and (d) Bonn potentials.

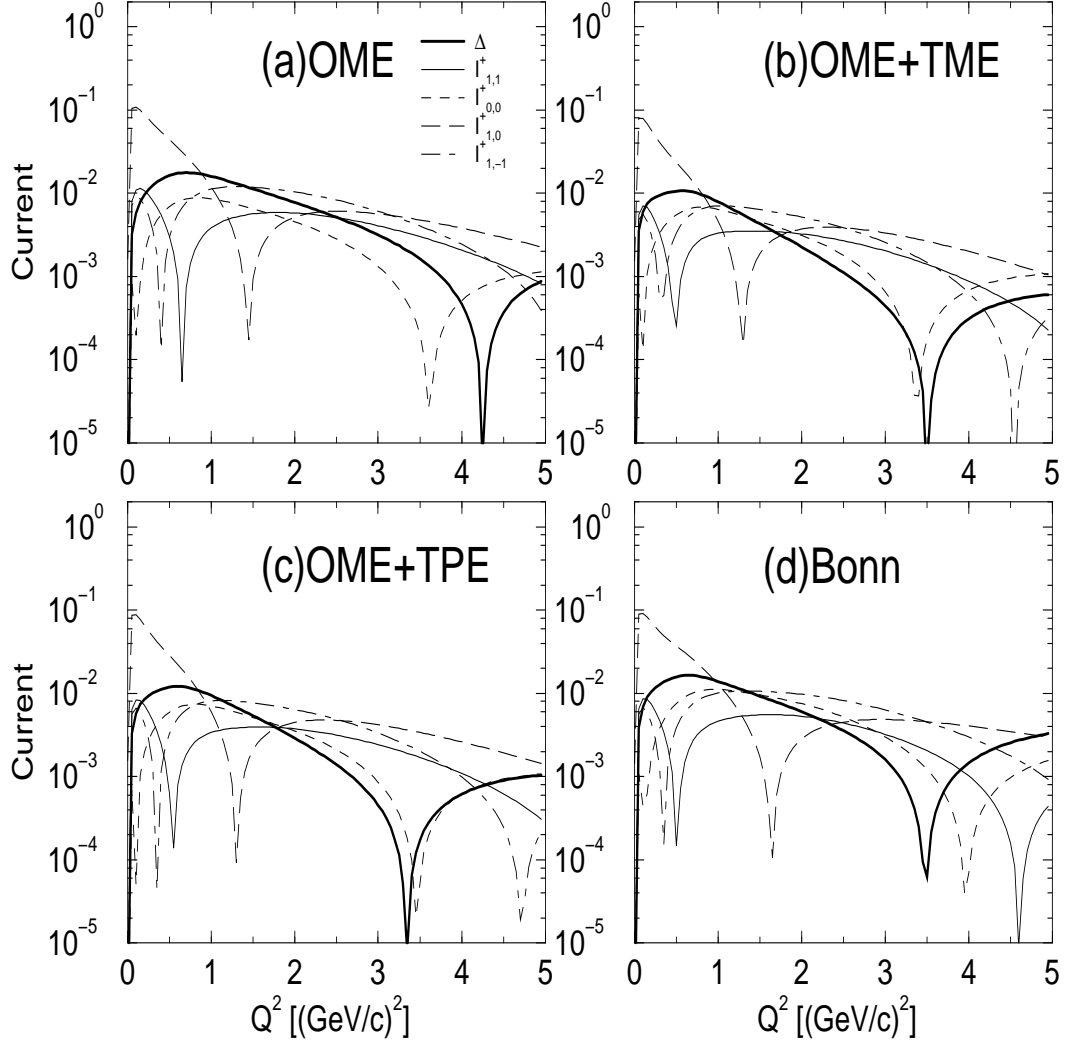


FIG. 12: The matrix elements of  $I_{(2)m'm}^+$ , the component of the electromagnetic current which multiplies the nucleon  $F_2$  form factor, calculated with the wave function from the (a) OME, (b) OME+TME, (c) OME+TPE, and (d) Bonn potentials.

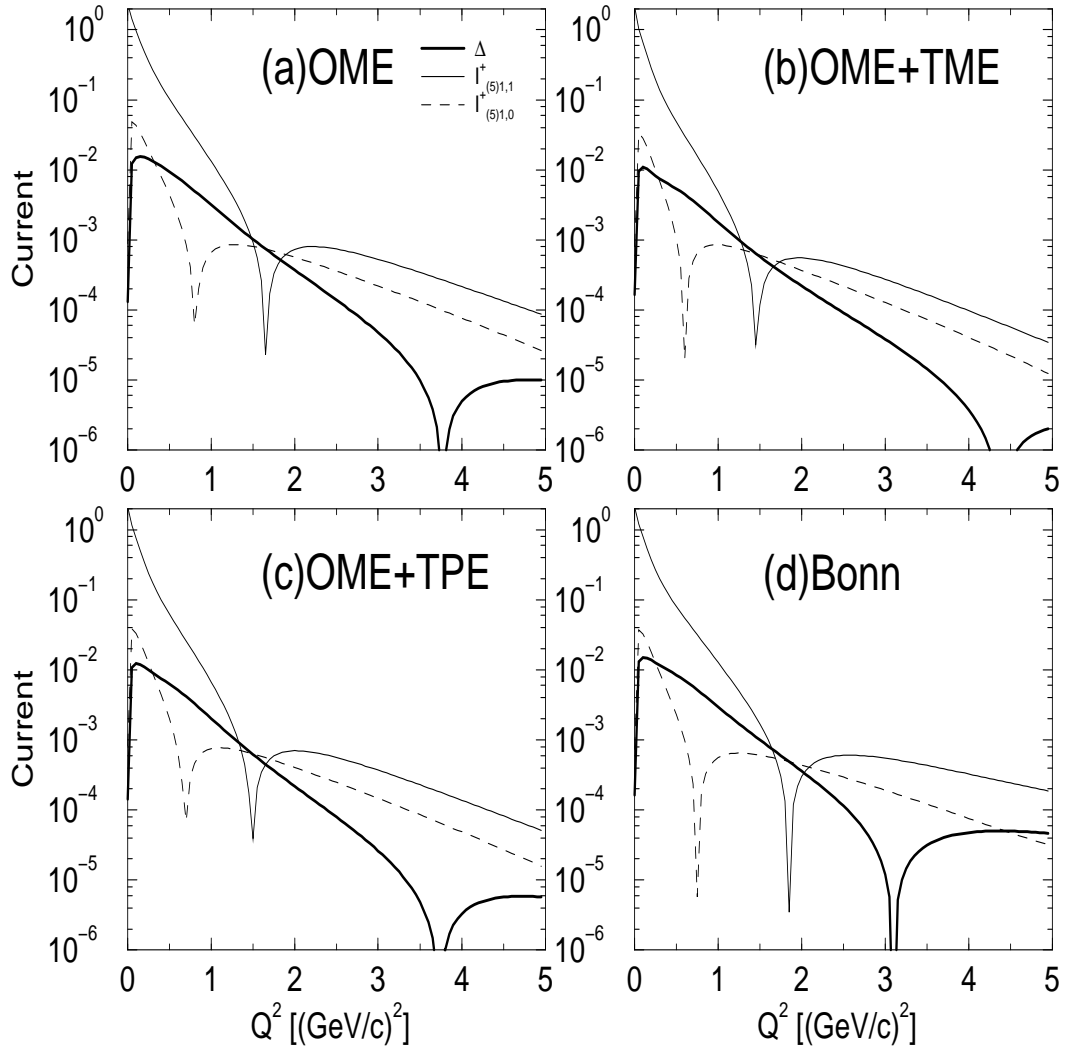


FIG. 13: The matrix elements of  $I_{(5)m'm}^+$ , the deuteron axial current including the nucleon axial form factor, calculated with the wave function from the (a) OME, (b) OME+TME, (c) OME+TPE, and (d) Bonn potentials.

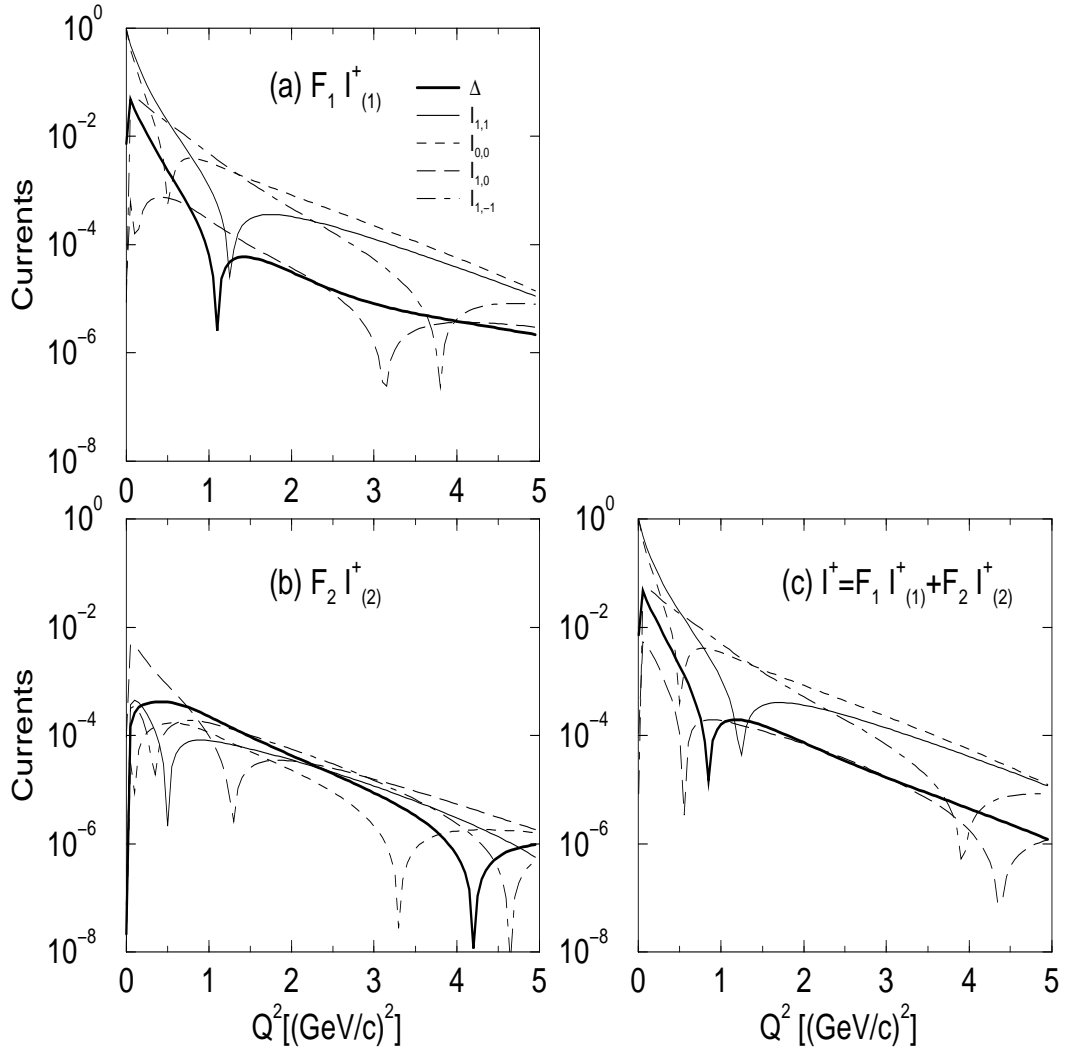


FIG. 14: The matrix elements for  $F_1 I_{(1)m'm}^+$ ,  $F_2 I_{(2)m'm}^+$ , and  $I_{m'm}^+$  calculated with the OME wave functions. The Gari:1985 nucleon isoscalar form factors are used for  $F_1$  and  $F_2$ .

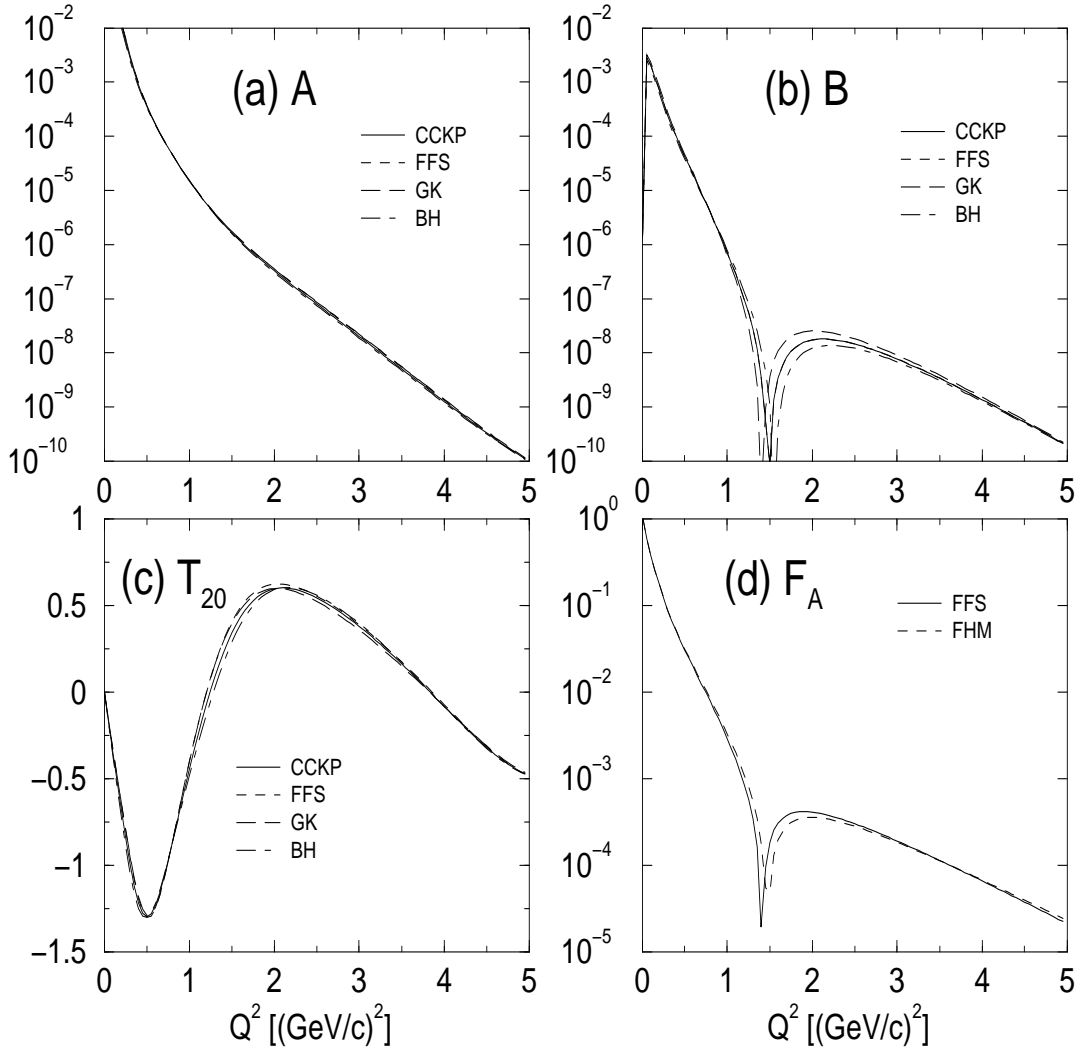


FIG. 15: The form factors  $A$ ,  $B$ ,  $T_{20}$ , and  $F_A$  calculated using the various choices of the “bad” matrix element. The OME wave function is used, along with the Lomon nucleon form factors for the electromagnetic form factors, and the Liesenfeld nucleon form factor for the axial form factor.

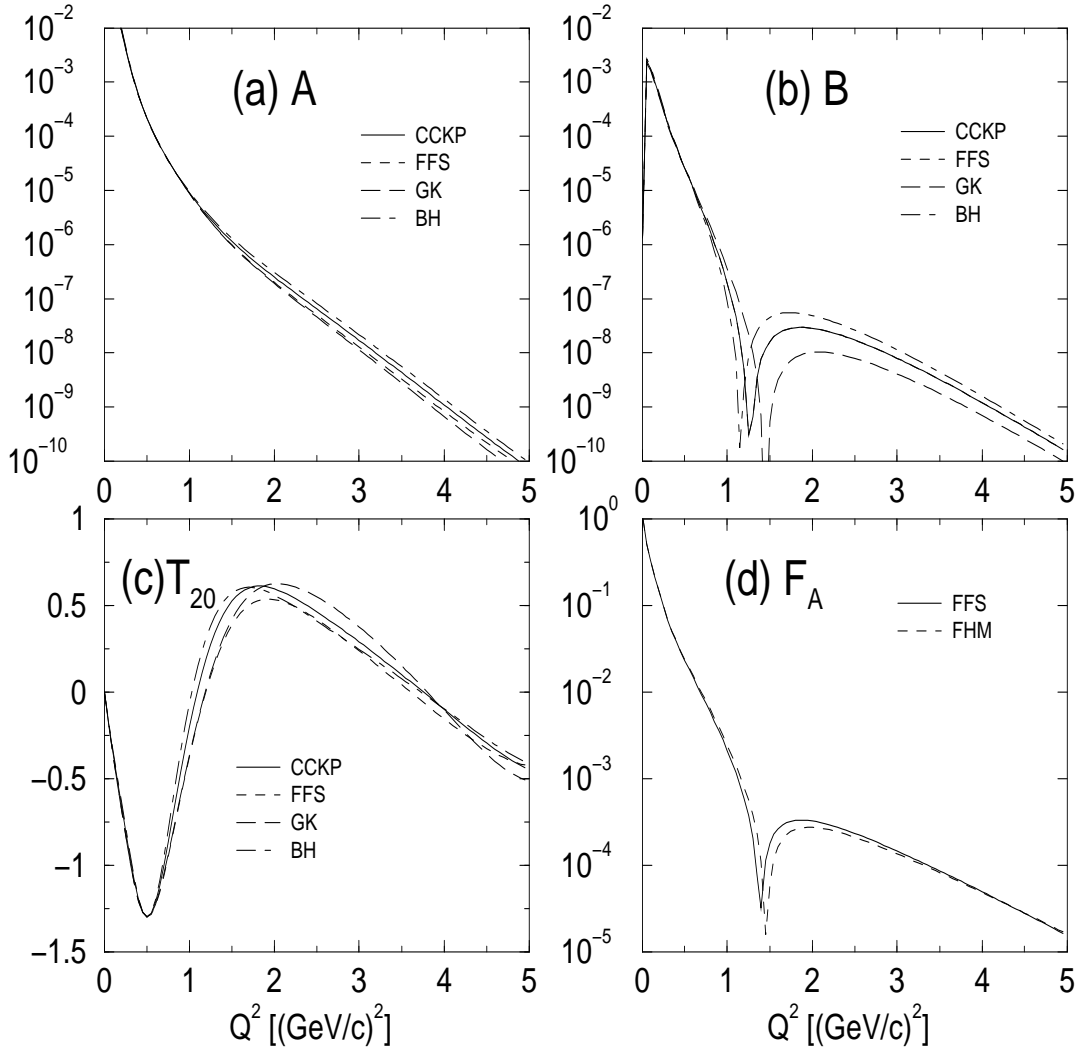


FIG. 16: The form factors  $A$ ,  $B$ ,  $T_{20}$ , and  $F_A$  calculated using the various choices of the “bad” matrix element. The definitions of the “bad” matrix elements are given in sections IV A 4 and IV B. The OME+TME wave function is used, along with the Lomon nucleon form factors for the electromagnetic form factors, and the Liesenfeld nucleon form factor for the axial form factor.

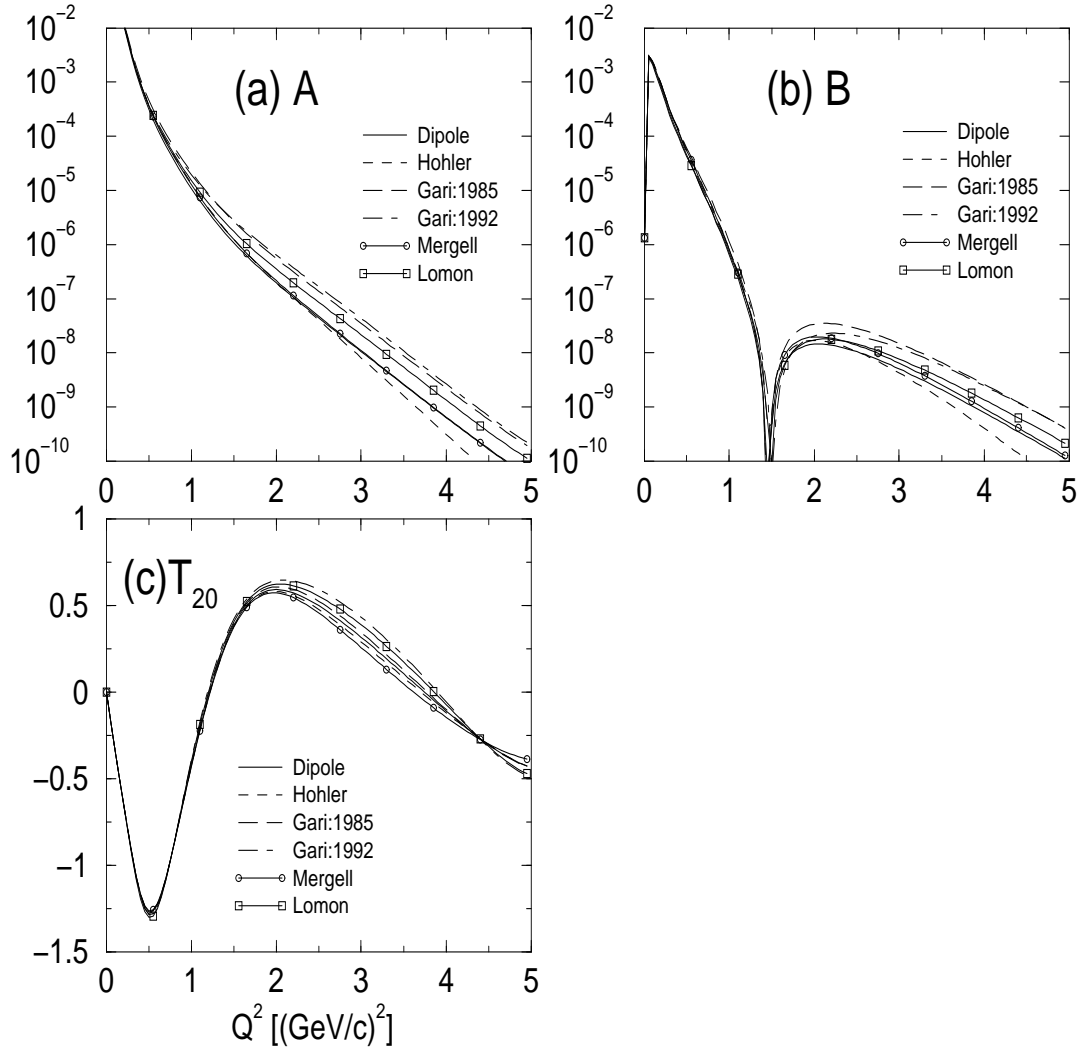


FIG. 17: The electromagnetic form factors  $A$ ,  $B$ , and  $T_{20}$  calculated using the various choices of the nucleon isoscalar form factors. The OME wave function is used, along with the FFS choice of the “bad” deuteron current matrix. The axial form factor is not shown since its dependence on different form factors is trivial.

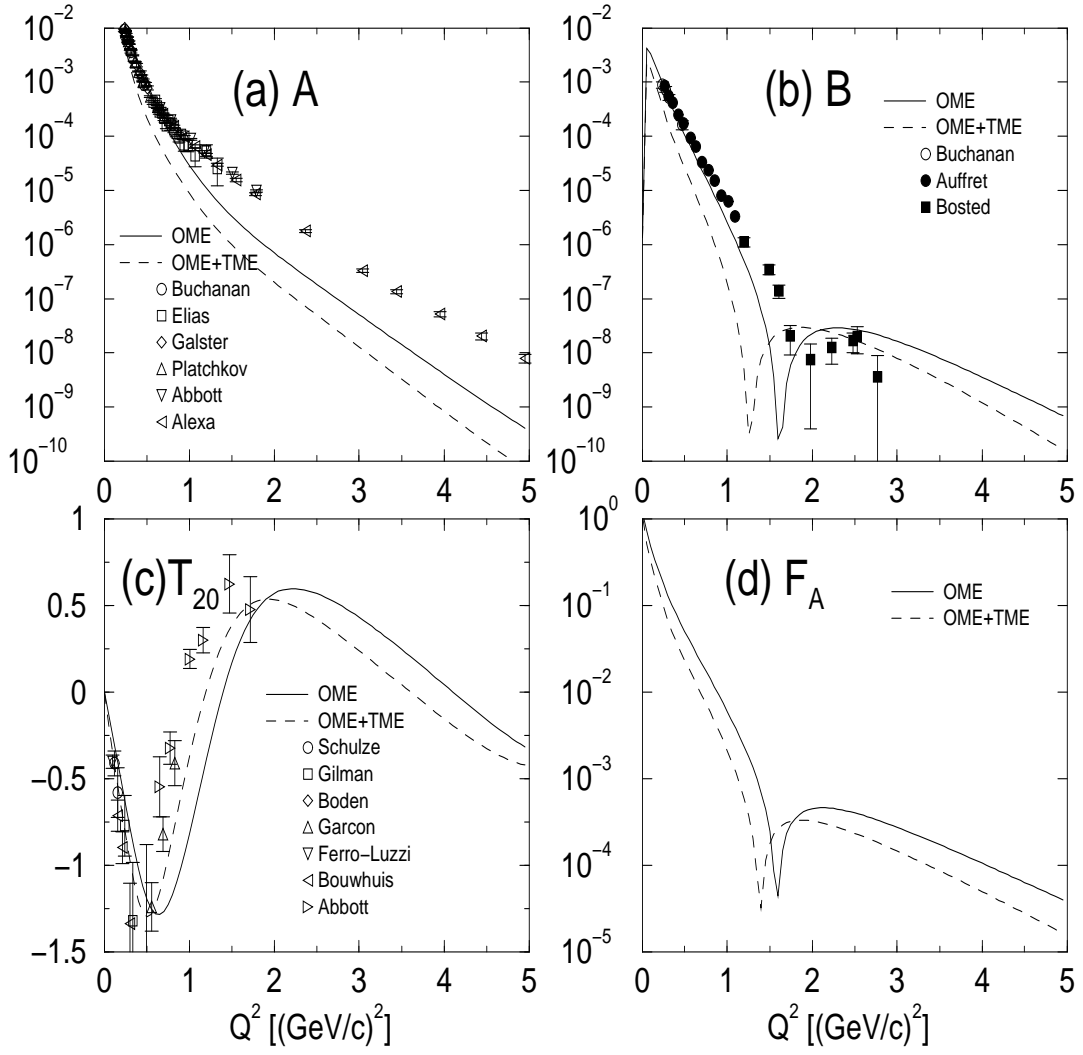


FIG. 18: The  $A$ ,  $B$ ,  $T_{20}$ , and  $F_A$  form factors for the OME and OME+TME potentials, along with data. See the accompanying text for an explanation of the data.